AD-A079 468 SCIENCE APPLICATIONS INC VIENNA VA F/G 7/4
SOFT X-RAY PHOTOEMISSION PROPERTIES FOR THE NEWLY MODELED MATER--ETC(U)
JAN 79 D J STRICKLAND, D L LIN DNA001-77-C-0209
UNCLASSIFIED SAI-102-78-029 DNA-4872F NL

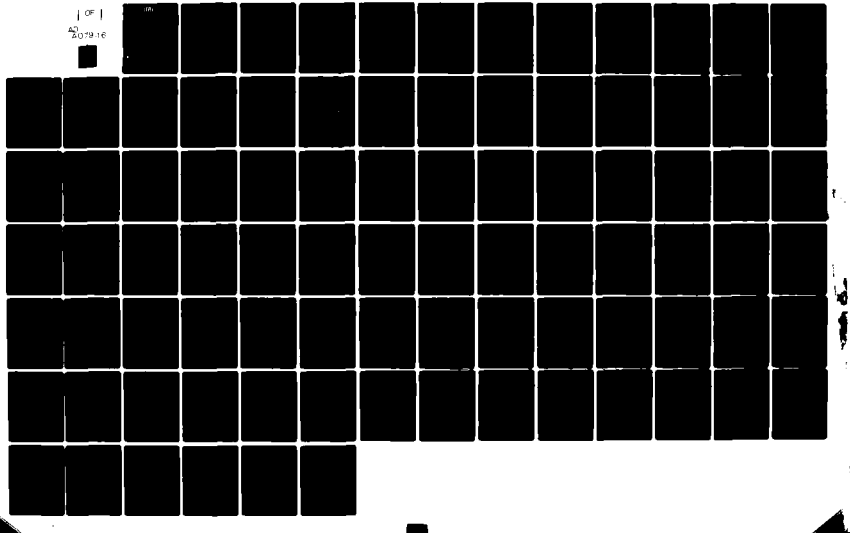

DNA 4872F

SOFT X-RAY PHOTOEMISSION PROPERTIES FOR THE NEWLY MODELED MATERIALS GOLD, SILVER, COPPER, AND CARBON

D.J. Strickland
D.L. Lin
Science Application, Inc.
8330 Old Courthouse Road, Suite 510
Vienna, Virginia 22180

3 January 1979

Final Report for Period 11 November 1977—3 January 1979

CONTRACT No. DNA 001-77-C-0209

APPROVED FOR PUBLIC RELEASE;
DISTRIBUTION UNLIMITED.

THIS WORK SPONSORED BY THE DEFENSE NUCLEAR AGENCY
UNDER RDT&E RMSS CODE B323077464 R99QAXEE50314 H2590D.

Prepared for
Director
DEFENSE NUCLEAR AGENCY
Washington, D. C. 20305

Destroy this report when it is no longer needed. Do not return to sender.

PLEASE NOTIFY THE DEFENSE NUCLEAR AGENCY, ATTN: STTI, WASHINGTON, D.C. 20305, IF YOUR ADDRESS IS INCORRECT, IF YOU WISH TO BE DELETED FROM THE DISTRIBUTION LIST, OR IF THE ADDRESSEE IS NO LONGER EMPLOYED BY YOUR ORGANIZATION.

(18) DNA, SBIE

UNCLASSIFIED

SECURITY CLASSIFICATION OF THIS PAGE (When Data Entered)

(19)

REPORT DOCUMENTATION PAGE	READ INSTRUCTIONS BEFORE COMPLETING FORM
1 REPORT NUMBER: DNA 4872F, AD-E300 638	2. GOVT ACCESSION NO. / 3. RECIPIENT'S CATALOG NUMBER
(6) 4 TITLE (and Subtitle): SOFT X-RAY PHOTOEMISSION PROPERTIES FOR THE NEWLY MODELED MATERIALS GOLD, SILVER, COPPER, AND CARBON	(9) 5 TYPE OF REPORT & PERIOD COVERED: Final Report, 11 Nov 77—3 Jan 79
	(14) 6 PERFORMING ORG. REPORT NUMBER: SAI-102-78-029
(10) 7 AUTHOR(s): D. J. Strickland, D. L. Lin	(15) 8 CONTRACT OR GRANT NUMBER(s): DNA 001-77-C-0209
9 PERFORMING ORGANIZATION NAME AND ADDRESS: Science Applications, Inc., 8330 Old Courthouse Road, Suite 510, Vienna, Virginia 22180	(12) 10 PROGRAM ELEMENT, PROJECT, TASK AREA & WORK UNIT NUMBERS: Subtask R99QAXEE503-14
11 CONTROLLING OFFICE NAME AND ADDRESS: Director, Defense Nuclear Agency, Washington, D.C. 20305	(11) 12 REPORT DATE: 3 January 1979
	13 NUMBER OF PAGES: 88
14 MONITORING AGENCY NAME & ADDRESS (if different from Controlling Office)	15 SECURITY CLASS (of this report): UNCLASSIFIED (17) E503
(12) 89	15a DECLASSIFICATION DOWNGRADING SCHEDULE

16 DISTRIBUTION STATEMENT (of this Report)

Approved for public release; distribution unlimited.

17 DISTRIBUTION STATEMENT (of the abstract entered in Block 20, if different from Report)

18 SUPPLEMENTARY NOTES

This work sponsored by the Defense Nuclear Agency under RDT&E RMSS Code B323077464 R99QAXEE50314 H2590D.

19 KEY WORDS (Continue on reverse side if necessary and identify by block number)

Soft X-Ray Photoemission
SGEMP

20 ABSTRACT (Continue on reverse side if necessary and identify by block number)

The work represents a continuation in our program to model soft x-ray photoemission for exploding wire radiator (EWR) sources incident on various materials. This program falls within the larger program SKYNET which is concerned with SGEMP effects for soft x-ray sources. Results are presented for four newly modeled materials - Au, Ag, Cu, and C. These results include the detailed atomic information required to model each material and

DD FORM 1 JAN 73 1473 EDITION OF 1 NOV 65 IS OBSOLETE

UNCLASSIFIED

SECURITY CLASSIFICATION OF THIS PAGE (When Data Entered)

AD-A111 539

20. ABSTRACT (Continued)

photoemission and backscatter results obtained with the code SXRP. In particular, photoemission spectra and total primary yields are presented for an EWR source incident on the four materials cited. Their measured counterparts are included for comparison. Some comparisons provide good agreement while others call for further investigation. For Au, additional spectra and yields are presented for sources narrow in energy to compare with available published data. The photon energy range considered is between 1 and 5 keV. Good overall agreement is obtained with the data.

TABLE OF CONTENTS

LIST OF FIGURES

LIST OF FIGURES (CONTINUED)

LIST OF FIGURES (CONCLUDED)

LIST OF TABLES

Section 1

INTRODUCTION AND SUMMARY

Over the past three years, SAI has developed and extensively exercised the SXRP code under the DNA-AFSC sponsorship to provide a rigorous capability in soft x-ray photoemission and provide results which can be directly compared with measured photoemission spectra and yields for exploding wire radiator (EWR) sources. The code and applications have been well-documented in a number of reports and papers.[1-8] Code validation has been an active part of the overall program and has met with considerable success.[2,4,6] Photoemission and electron backscatter results have been obtained for the materials:

- aluminum (Aℓ),
- aluminum oxide ($Aℓ_2O_3$), and
- silicon dioxide (SiO_2).

Sources considered for photoemission have included an OWL II´ EWR source, line sources, blackbody spectra, and a 50 kVp Bremmstrahlung spectrum generated by Bradford.[9] Electron backscatter calculations have been carried out for incident electron energies in the low keV range.

The above work, as well as that reported herein, has been undertaken in support of DNA's SKYNET program which is concerned with satellite SGEMP effects caused by soft x-ray sources. The three materials listed above are but part of a larger set being actively investigated in the SKYNET program and more generally in various programs concerned with SGEMP and spacecraft charging effects. Examples of other materials of interest are gold and carbon dominated dielectrics, such as Kapton. To address this larger set of materials, work during the given contract period was undertaken on four new materials:

- gold (Au),
- silver (Ag),
- copper (Cu), and
- carbon (C).

This effort, in some aspects, represented a significant departure from earlier work. The new materials, especially Au, are considerably more complicated in their atomic structure (with the exception of C) and there is generally less information available on the needed material parameters compared to the three materials previously investigated. Consequently, a larger fraction of the effort had to be directed to the specification of these parameters. This will be evident in the sections to follow in which we present a considerable amount of information on the material models themselves.

Gold was the first new material we addressed in this work. A disproportionate amount of time had to be spent on this material since an extension of current capabilities was required due to the high-Z nature of Au and, as noted above, due to the need to generate certain types of parameters for the first time. The primary limitation in capabilities centered on our description of elastic scattering. The specification of the differential cross section, while adequate for a low-Z material like Al, proved unacceptable for Au having a Z-value of 79. To correct this situation, we carried out an investigation of the atomic screening potential itself with consideration given to solid state effects on this potential. This work was begun under a previous contract and a further discussion may be found in the associated final report.[6]

Gold appears to have more photoemission and electron backscatter associated with it than the other three new materials. This provides another reason for the greater emphasis on this material in addition to considering it for extending of our capabilities in modeling materials. Several results will be presented and compared with published data in addition to those for the OWL II´ EWR source which is the source of prime concern at this time in the SKYNET program.

The objectives in this work may be listed as follows:

- Specify material models for Au, Ag, Cu, and C to rigorously investigate soft x-ray photoemission.

- Validate the models:
  - — compare to other values of material model parameters,
  - — compare transport results with measurements:
    - -- photoemission yields,
    - -- electron backscatter yields.
- Provide a basic understanding of photoemission for soft x-ray sources incident on the new materials.
- Directly support the SKYNET program through comparisons of the calculated photoemission spectra and yields with measurements of these quantities for the OWL´II EWR source.

Overall, these objectives were *met* with good success although more work should be done on material model validation for Ag, Cu, and C. We were unable to find data for these materials to the extent available for Aℓ and Au. Thus, photoemission results for these materials are necessarily more uncertain although we believe the larger uncertainty is primarily in the yield and not in the overall structure of the emission spectrum or in our understanding of the important mechanisms operating.

We may summarize our results as follows:

- The needed material models for a rigorous description of SXRP have been specified for the first time for Au, Ag, Cu, and C.

- For Au, photoemission and electron/backscatter results were obtained for sources narrow in energy between 1 and 5 keV and compared with published data. Good agreement was achieved for both photoemission and electron backscatter.

- Photoemission spectra and yields were obtained for an EWR source incident on each of the newly modeled materials. The description for Au should be good based on the excellent agreement noted above. Less confidence can be placed on the descriptions for Ag, Cu, and C although we expect the yields to be accurate to better than 50% and that, in general, the spectral shapes will not change significantly upon more detailed analyses.

- The above results were compared with the spectrometer data of Bernstein[10] and results by Fromme, et al.[11] deduced from back-biased diode data:

  — Spectral shapes agree reasonably well between the calculations and Bernstein's data. An exception to this occurs for Au between 1 and 2 keV. The calculated spectrum is noticeably higher in this region.

  — Spectral shapes do not agree well at all between the calculations and the Fromme, et al. results. The diode data cannot be used to provide spectral information with a reasonable confidence level as demonstrated in a previous report and further discussed in this report for Au in Section 4.

  — Total yields (for electrons above $\sim$0.1 keV) agree to within a factor of two. The calculated yield for Au, which should be accurate based on above-mentioned comparisons, is $\sim$50% above Bernstein's value. For Ag, the calculated yield is about half, while for C it is about the same as Bernstein's value. Further work is planned for Ag which may resolve the present discrepancy.

Section 2

GOLD

In this section, we discuss our first results for photoemission and electron backscatter from Au using the SXRP code. We also present, for the first time, a detailed atomic model for Au which is required by the code. The emphasis will be on a calculation of the photoemission spectrum and the total yield for an EWR source incident on Au and comparison of these quantities with those deduced by Fromme, et al.[11] from biased diode data and measured by Bernstein[10] with a magnetic spectrometer. A similar comparison has previously been made for Aℓ.[4]

2.1 ATOMIC MODEL FOR GOLD

Gold is a particularly difficult material to model for low energy electron transport calculations since there are many subshells for which the photoionization cross sections, electron IMFP's, and Auger energies and yields must be specified. Prior to this work, much of the needed information did not exist. A major part of the work thus being reported here has been directed to specifying the needed input parameters.

Table 1 shows the atomic shells and binding energies explicitly treated in our calculations. The L and K shells are not included since their binding energies are

TABLE 1. ATOMIC SHELLS OF Au TREATED IN THIS WORK AND THEIR BINDING ENERGIES

SHELLS	BINDING ENERGIES (keV)
M_1	3.425
M_2	3.150
M_3	2.743
M_4	2.291
M_5	2.206
N	0.083
O_{23}	0.052
O_{45}	0.008

above 10 keV, the upper limit to the energy range of current interest. All electrons through the O shell are treated as bound electrons. Gold also possesses a P shell in the atomic form containing one electron. This electron has been assigned to the conduction band in our formulation.

Figure 1 shows the photoabsorption coefficients corresponding to Table 1. The O shell and N shell cross sections are based on the work of Haensel, et al.[12] and Manson,[13] respectively. The tabulations of Hubbell[14] and Biggs and Lighthill[15] were used to provide the total M shell cross section. The specification of the subshell cross sections was made by us with the assistance of the binding energies given in Table 1.

Figure 2 shows the inelastic IMFP's, both for electron impact ionization of the inner shell electrons and for ionization and plasmon excitation of the conduction band electrons. To our knowledge, such information for the inner shells of Au has not been specified before. Also included in the figure are data giving the measured total inelastic IMFP.[16-21] The inner shell IMFP's were obtained by us using a formula which directly relates the IMFP to its corresponding photoabsorption coefficient. The coefficients in Figure 1 were used to obtain the given IMFP's. A brief discussion of the method appears in the 1978 RADC Final Report, together with its application to the K and L shells of Aℓ.[6] Good agreement was achieved with more rigorous results by Ashley, et al.[22] providing some confidence that the method is giving a good approximate representation to the IMFP as long as the photoabsorption coefficient is reasonably well specified. The plasmon and conduction band ionization IMFP's were obtained by us using the

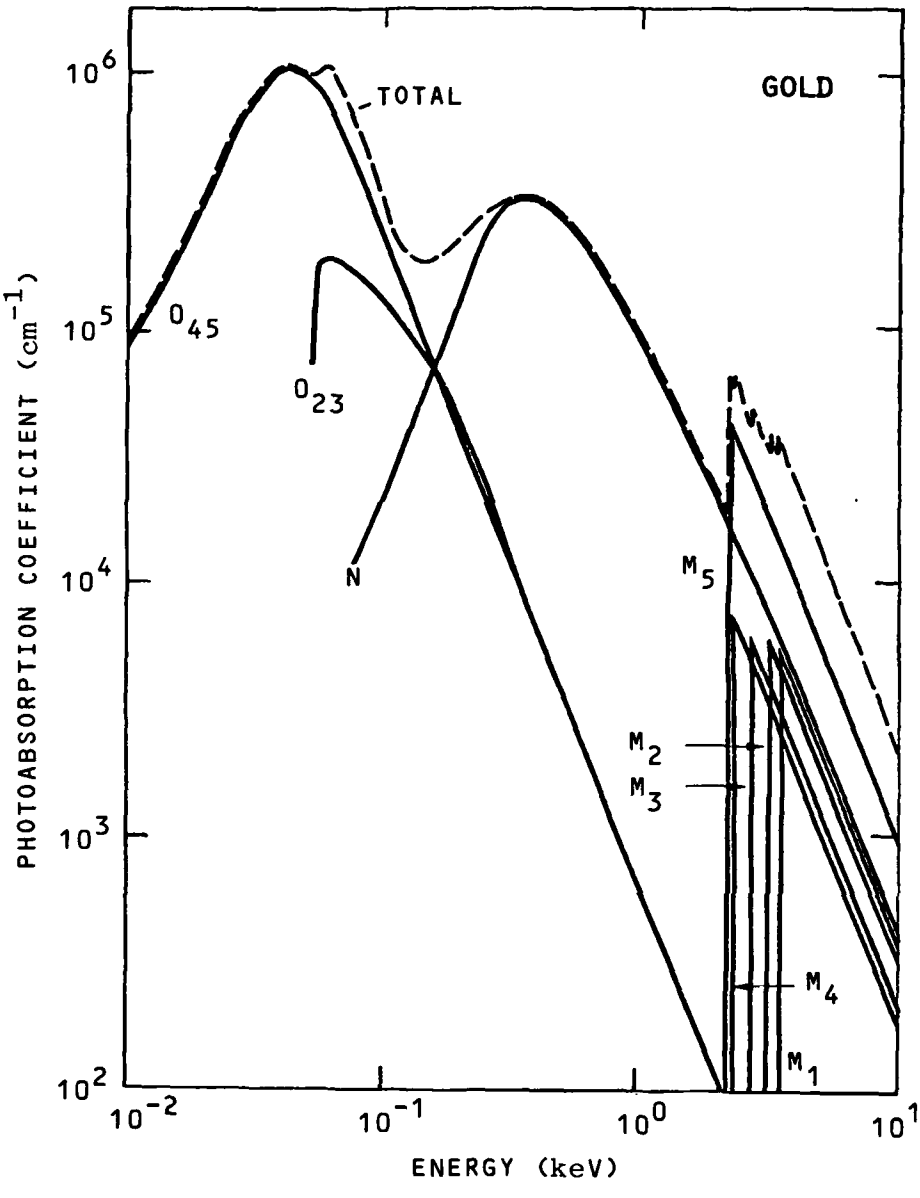

FIGURE 1. Photoabsorption Coefficients for Au.

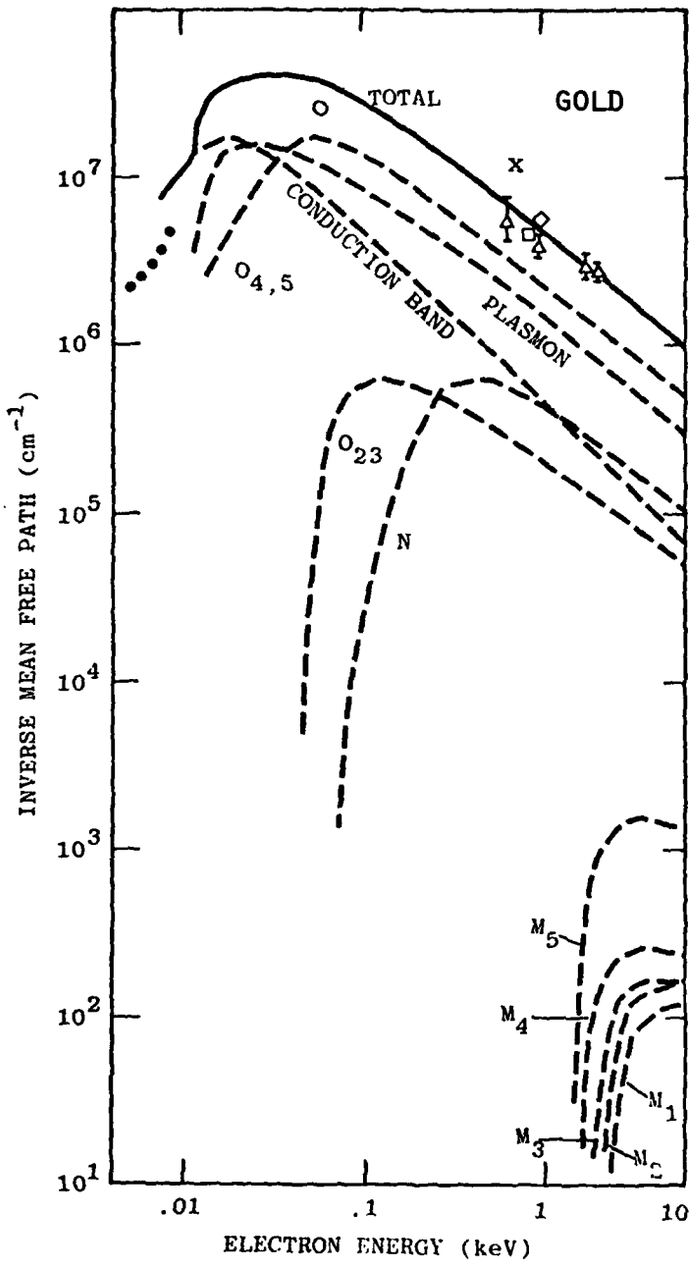

FIGURE 2. Inelastic Inverse Mean Free Paths for Au.

The data are as follows: ● Kanter,[16] ○ Palmberg, et al.,[17] △ Klasson, et al.,[18] □ Baer, et al.,[19] ◇ Henke,[20] and x Powell.[21]

ORNL methodology[22] which deals with the dielectric response function in solids. To obtain the given results, a conduction band electron density given by one electron per atom (the P electron) was used. This corresponds to a Fermi energy of 5.5 eV.

Figure 3 shows the elastic IMFP, together with the screening parameter η which specifies it. The sum of all considered inelastic IMFP's is also included for comparison with the elastic IMFP. The elastic differential IMFP is given by:

$$K_{elas}(E,\theta) = \frac{nZ^2e^4}{v^2p^2} \frac{1}{(1 - \cos\theta + 2\eta)^2} , \quad (1)$$

where θ is the scattering angle, n is the material number density, Z is the atomic number, and v and p, respectively, are the velocity and momentum of the incident electron. The screening parameter η is given by:

$$\eta(E) = 4.3\ Z^{2/3} \frac{\eta_c}{E} , \quad (2)$$

where E is in eV and η_c is a function of the screening potential. The screening potential in conducting solids can be adequately represented by a single Yukawa potential which leads to constant η_c. We choose the value $\eta_c = 3.2$, based on considerations given by Nigam, et al.[23] As will be seen, this choice gives good agreement with measurements for both backscatter and photoemission yields. Excellent agreement with measurements for the given η_c has previously been obtained for Aℓ.[6]

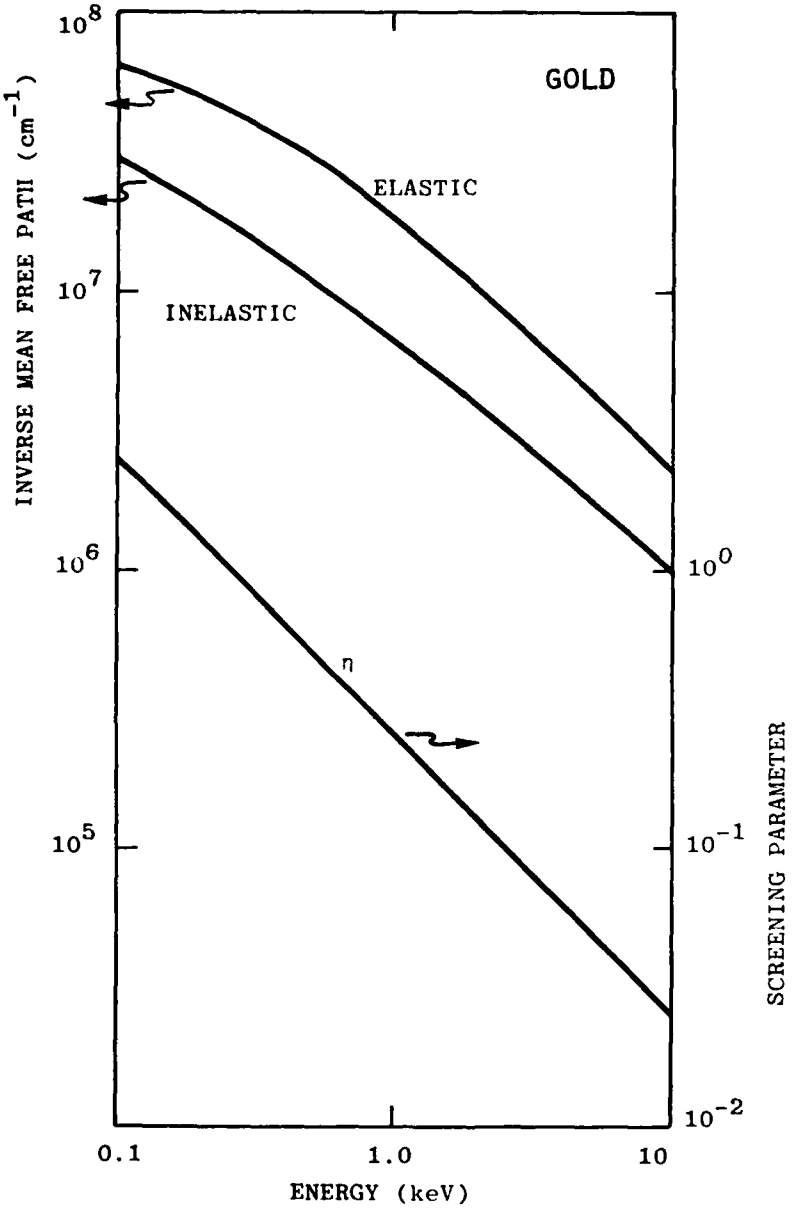

FIGURE 3. Total Elastic Inverse Mean Free Path, Its Corresponding Screening Parameter η, and Total Inelastic Inverse Mean Free Path for Au.

Our model for the relevant Auger spectroscopy is given in Table 2. The model serves its one basic requirement — the proper accounting of the bulk of potential energy of the inner shell vacancies. For most transitions shown in the table, several Auger lines exist although one will usually be dominant.[24] The energy shown is the energy of the dominant line within a group. For Au, the Auger spectroscopy treatment in the SXRP code is considerably more complicated than indicated by Table 2. Each of the M subshells is treated explicitly which requires consideration of intra-, as well as inter-shell transitions. A more detailed description of the applied spectroscopy for Au appears in the 1978 RADC Final Report.[6]

2.2 PHOTOEMISSION FROM Au FOR AN EWR SOURCE

The results to follow are the first we have obtained for Au using the SXRP code. For this reason, the initial runs were made for selected narrow Gaussian photon and incident electron sources so that the calculated photoemission and electron backscatter yields could be compared with published data. In this way, we are able to determine if our material model for Au is reasonable for such applications as predicting the photoemission spectrum and the yield for an EWR source. Since this is the application of interest in this subsection, results will be presented for an EWR source next. This will then be followed by photoemission and backscatter results for narrow Gaussian sources to demonstrate that, in fact, we do have a good working model for Au in the low keV range.

TABLE 2. TRANSITIONS, ENERGIES, AND YIELDS FOR AUGER ELECTRONS IN Au

TRANSITION	ENERGY	YIELD
MNN	2.11	0.35
MNN	2.02	0.52
MNN	1.77	0.13
NNO	0.239	0.11
NOO	0.069	0.89

The representation of the EWR spectrum used to do the calculations is shown in Figure 4. This spectrum is based on crystal spectrograph data appearing in a 1977 Physics International report by Nielson,[25] and has been previously used to predict the photoemission from Aℓ.[4] The narrow feature peaking at 1.65 keV contains ∿50% of the energy and is used in the calculations in place of the two strong emission lines appearing in the data at 1.6 and 1.7 keV. Some variation has been seen to occur from shot to shot in the energy content of these lines relative to the rest of the spectrum. For example, Nielson reports values of 65% and 50% for the two shots (2952 and 2953) discussed in connection with the spectrograph data. It is important to know how sensitive the photoemission spectrum and total yield are to such a variation, especially for direct comparisons of the calculated and measured values of these quantities as will follow. To address this point, we have obtained results for two EWR spectra in addition to the one shown in Figure 4. For the one case, the 1.65 keV feature contains ∿25% of the energy, while for the other case, the value is ∿75%. The resulting photoemission spectra will be presented in the next subsection. For comparison with the measurements, we will use the EWR spectrum which contains 50% of the energy in the 1.65 keV feature. Variation of the energy content in this feature does affect the shape of the spectrum, but, interestingly enough, has virtually no effect on the total yield when given in units of emission current per unit incident fluence (e.g., coul/cal). Thus, the calculated yield values we quote are independent of the actual strength of the 1.65 keV feature. This will be discussed further in the next section.

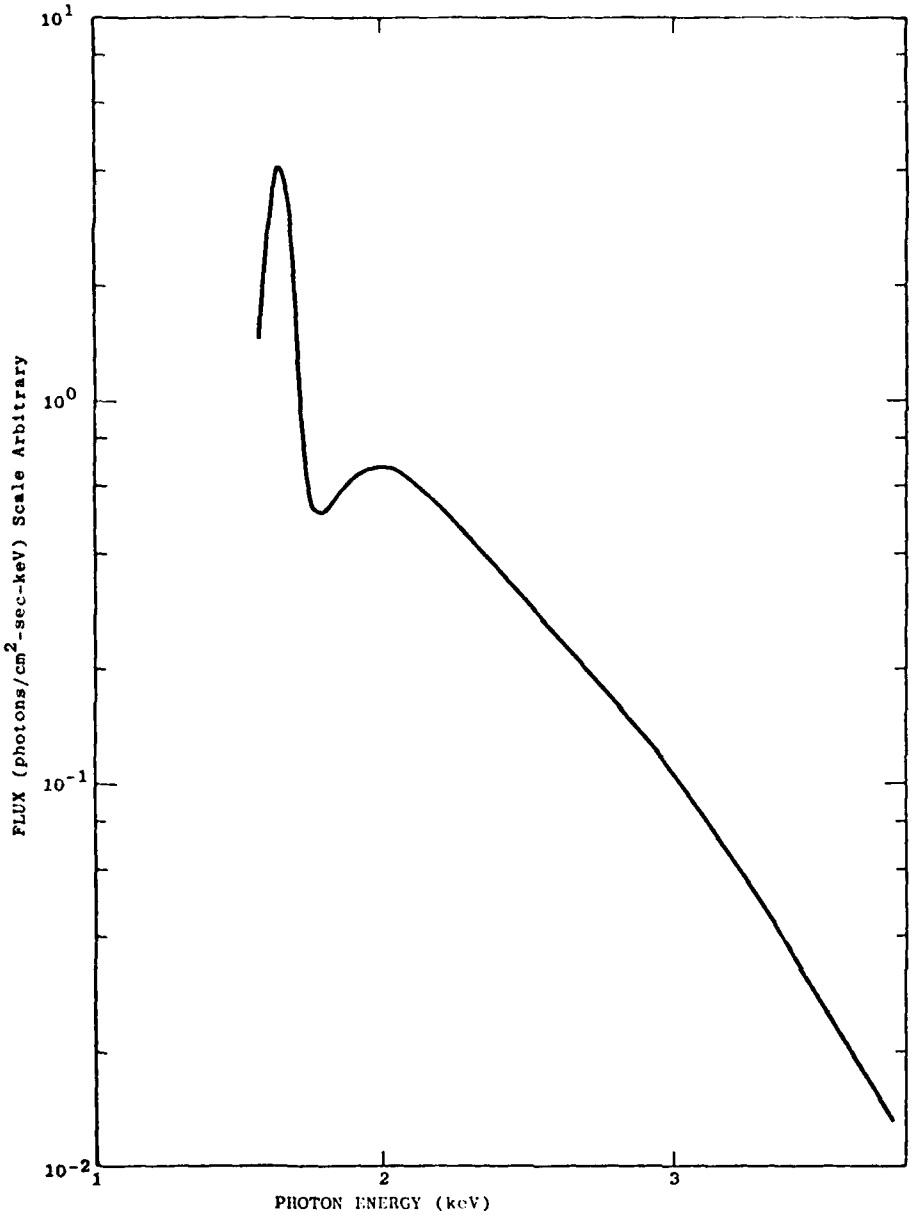

FIGURE 4. Continuum Representation of an EWR Source.

The calculated photoemission spectrum for Au is shown in Figure 5, together with Bernstein's spectrometer measurements[10] and the spectrum by Fromme, et al. inferred from back-biased diode data.[11] The total yields are included in the figure, as well as in Table 3, which are 3.2×10^{-5} coul/cal (SXRP), 2.1×10^{-5} coul/cal (Bernstein), and 1.9×10^{-5} coul/cal (Fromme, et al.). The SXRP value is consistent with the value one would obtain by folding the EWR photon spectrum with the observed total photoemission yield curve versus hν (see Figure 10).

The spectral shapes in Figure 5 are significantly different from one another as was initially observed for Aℓ.[4] We have previsouly demonstrated that the diode data of Fromme, et al., together with their analysis, cannot provide a realistic spectrum.[4] Bernstein's spectrum shows reasonable agreement with the calculated spectrum at the high and low energy ends. The calculation, however, predicts considerably more emission in the middle region due to N shell photoelectrons and MNN Auger electrons. This condition persists over the range of uncertainty and variability in the EWR photon spectrum which will be demonstrated in the next section. We will now discuss in some detail the overall features of the spectrum. To aid in this discussion, we show the separate photo- and Auger contributions to the calculated spectrum in Figure 6.

The features peaking at 2.1, 2.0, 1.8, and 0.24 keV are due to MNN and NNO Auger electrons (see Table 2). Photons above 2.2 keV contribute to the MNN Auger emission. The underlying continuum beginning at high energies and the strong peak at 1.5 keV reflect the EWR spectrum and are due primarily to N photoelectrons (see the N shell photoabsorption coefficient in Figure 1). The fall-off below the

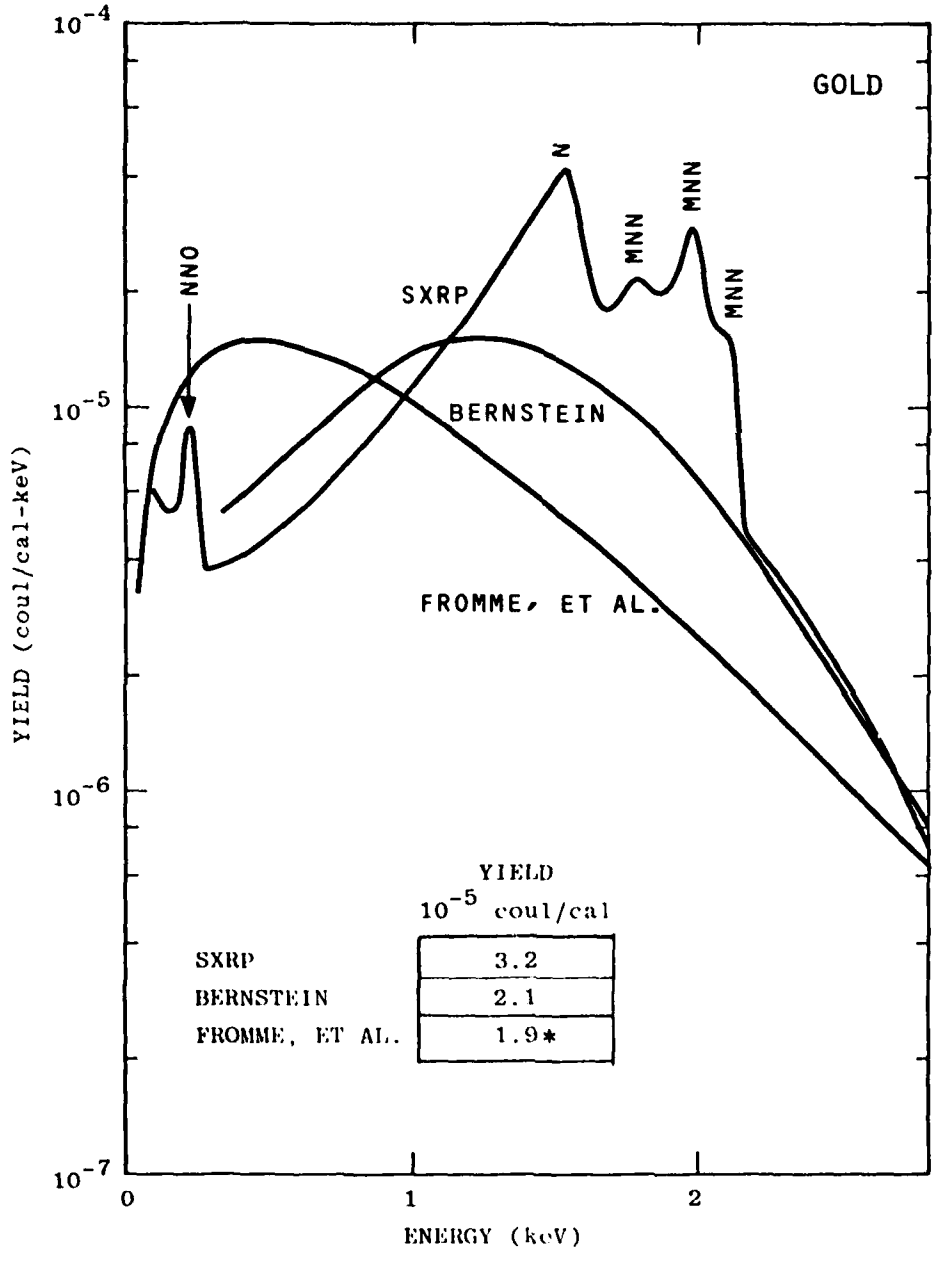

FIGURE 5. Calculated and Measured Photoemission Spectra for an EWR Source Incident on Au.

*Value initially reported. Later value is 2.1.

TABLE 3. ELECTRON BACKSCATTER AND PHOTOEMISSION YIELDS FOR SELECTED SOURCES INCIDENT ON Au

SOURCE		SXRP el/ph	SXRP coul/cal	MEASUREMENT el/ph	MEASUREMENT coul/cal
e^-	2.0 keV	0.53 el/el		0.50 el/el [28]	
hν	1.0 keV	1.56×10^{-2}	6.48×10^{-5}	SEE FIGURE 10.	
hν	2.0 keV	9.7×10^{-3}	2.0×10^{-5}	SEE FIGURE 10.	
hν	2.5 keV	2.7×10^{-2}	4.5×10^{-5}	SEE FIGURE 10.	
hν	5.0 keV	1.62×10^{-2}	1.35×10^{-5}	SEE FIGURE 10.	
hν	EWR	1.5×10^{-2}	3.2×10^{-5}	9.5×10^{-3} [10] 8.6×10^{-3} [11]	2.1×10^{-5} [10] 1.9×10^{-5} [11]

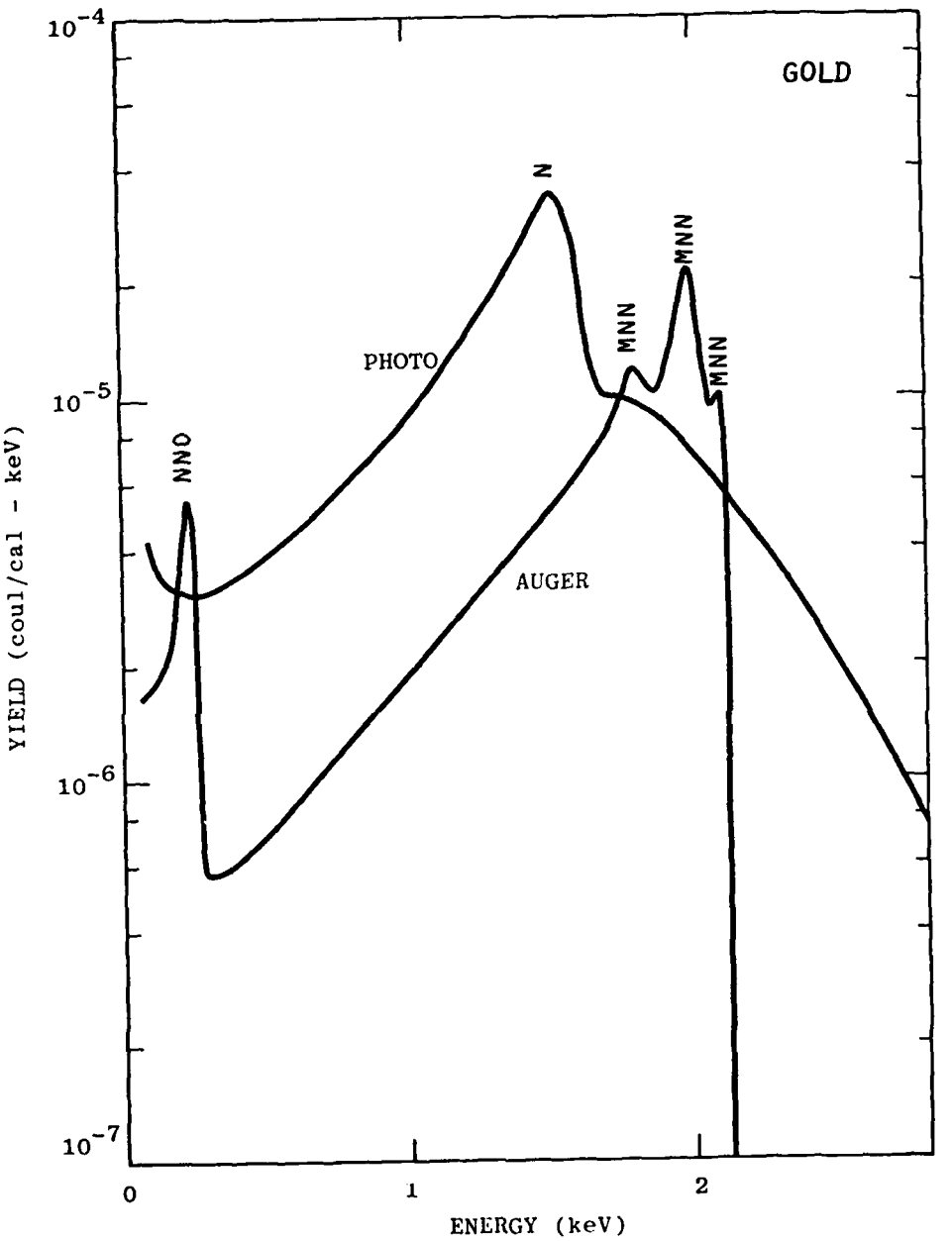

FIGURE 6. A Breakdown of the Calculated Photoemission Spectrum for an EWR Source Incident on Au into Its Photoelectron and Auger Electron Components.

1.5 keV peak is governed by the scattering and energy loss of the electrons originating above 1.5 keV. At the lowest energies, the rise in the spectrum is due to the production of secondary electrons and M photoelectrons. The MNN Auger electrons contribute 30% to the total photoemission yield.

The photoemission spectrum is, in general, very sensitive to the choice of material. This is particularly true for an EWR source incident on Aℓ and Au, as illustrated in Figure 7. The Aℓ spectrum was previously calculated with the SXRP code and has been thoroughly discussed.[4] The Au spectrum is noticeably harder with a mean energy of 1.4 keV compared with a mean energy of 1.0 keV for Aℓ. The yield for Au is also more than twice that for Aℓ. At high energies ($\gtrsim$ 2.2 keV), Au emits much more strongly due to its photoabsorption coefficient being nearly an order of magnitude larger than that for Aℓ at these energies. The rest of the differences may be explained in terms of locations of edges with respect to the photon spectrum and, as above, in terms of relative magnitudes of the photoabsorption coefficients.

Prior to obtaining the EWR photoemission spectrum for Au with the SXRP code, a representation of this spectrum was obtained using a recently developed empirical photoemission code.[6] The code is based on the Schaefer-Burke empirical model for line sources,[26,27] but generalizes the model to handle an arbitrary photon spectrum. Figure 8 provides a comparison of the SXRP spectrum with the empirical spectrum. Significant differences exist as was the case for Aℓ. A detailed discussion of the causes for the overall difference has been given for Aℓ.[6] Briefly, the SXRP code provides a detailed description of scattering whereas the assumption is made in the empirical code that electrons move

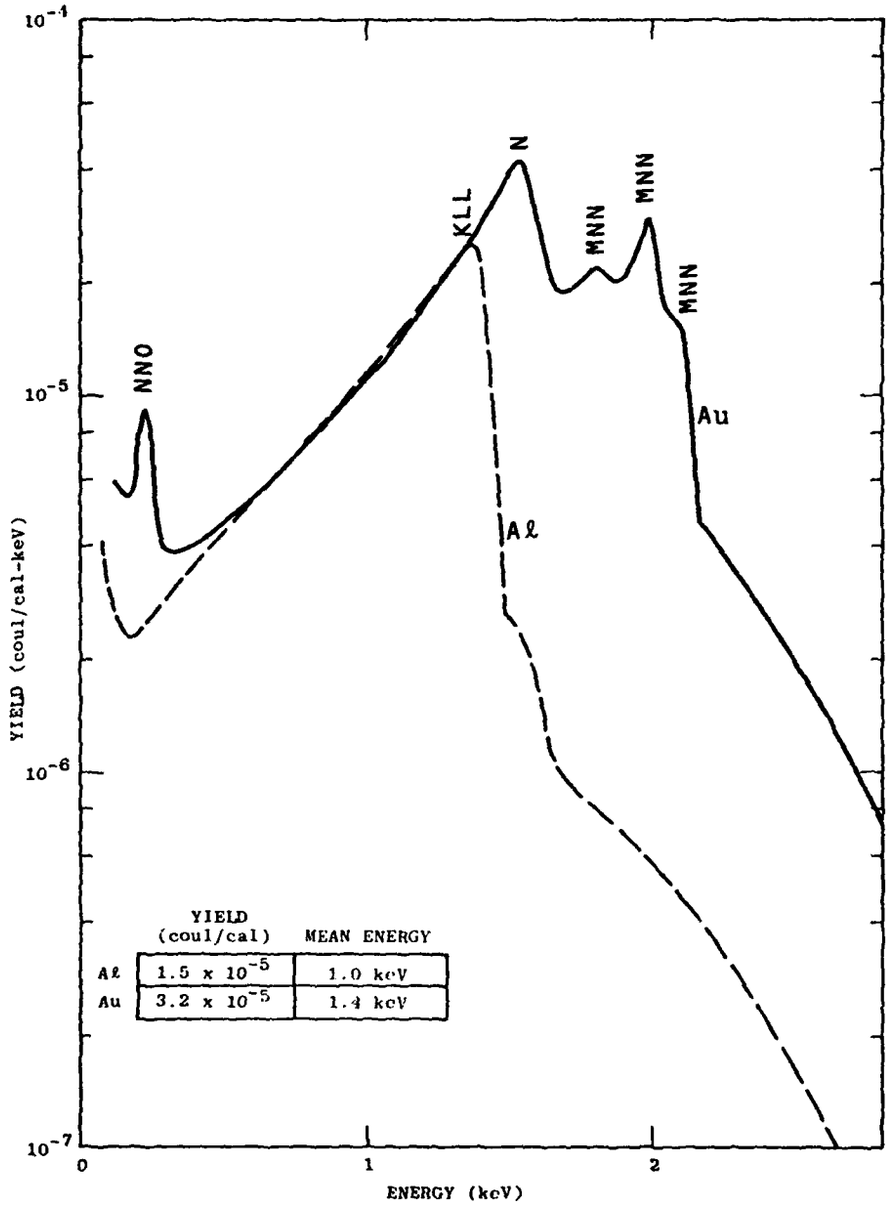

FIGURE 7. Calculated Photoemission Spectra for an EWR Source Incident on Aℓ and Au.

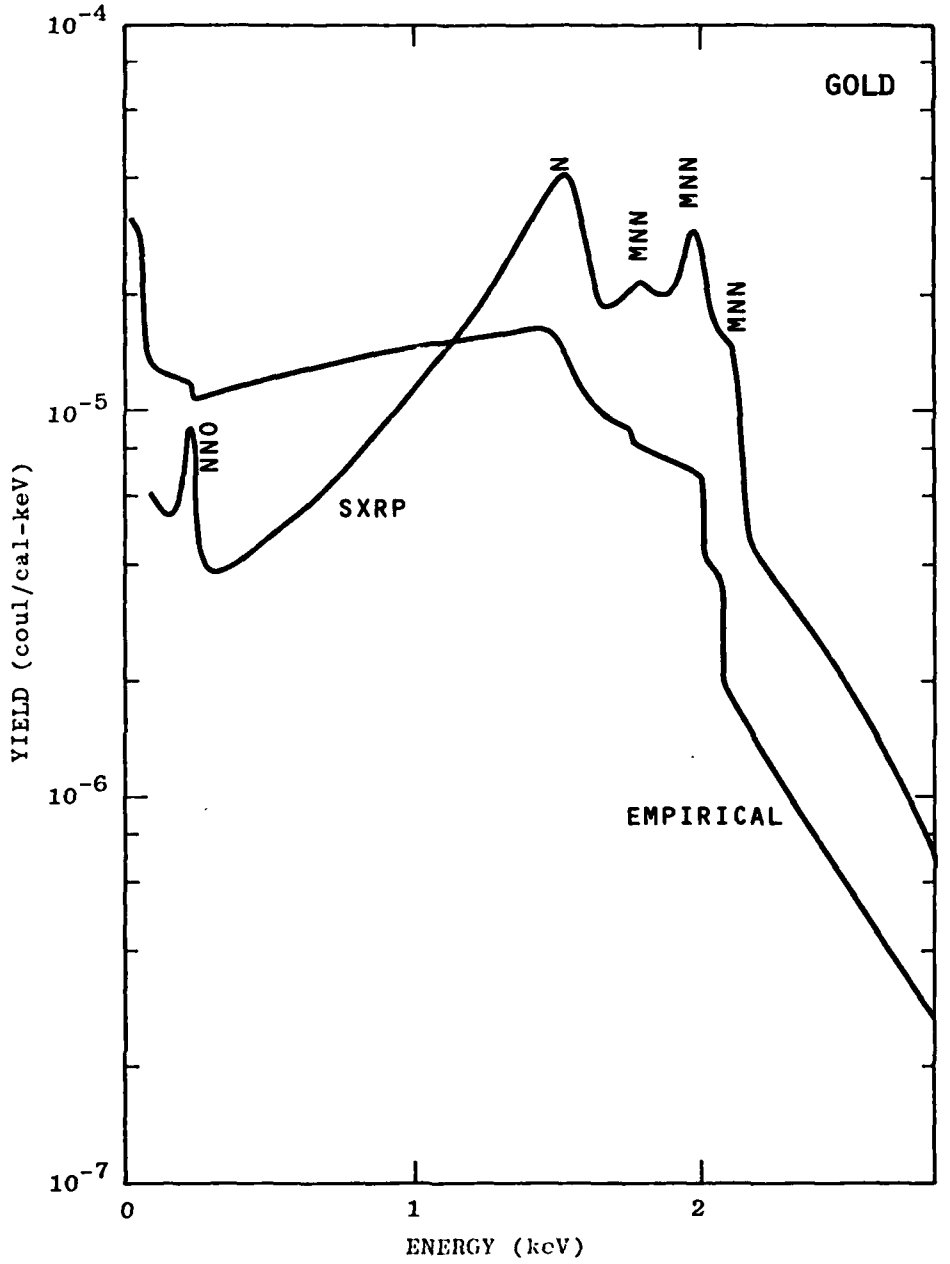

FIGURE 8. SXRP Calculated and Empirically Calculated Photoemission Spectra for an EWR Source Incident on Au. Both Spectra Give the Same Total Yield.

in straight line trajectories from creation to escape. The differing description in scattering is an important source of the spectral differences. Another source involves the treatment of energy loss. The SXRP code utilizes a discrete energy loss description whereas the empirical code utilizes a continuous energy loss description. Although the empirical model does not provide an accurate photoemission spectrum, it has been quite successful in predicting the total yield for various materials.[26]

2.3 SENSITIVITY OF THE PHOTOEMISSION FROM Au TO VARIATIONS IN THE EWR SPECTRUM

As discussed in the previous section, we have performed calculations for three representations of the EWR spectrum. These spectra, which will be referred to as Spectra 1-3, contain 25%, 50%, and 75%, respectively, of their energy in the narrow 1.65 keV feature. Spectrum 2 was previously presented in Figure 4. Spectra 1 and 3 are obtained from Spectrum 2 by scaling the 1.65 keV feature by the factors 1/3 and 3, respectively.

The resulting photoemission spectra are shown in Figure 9, while total yield information appears in Table 4. For each spectrum, the electron emission below 1.7 keV is due primarily to the photons within the 1.65 keV feature. In discussing the differences in Figure 9, it should be kept in mind that each spectrum in el/cm^2-sec-keV has been divided by its respective photon fluence in cal/cm^2-sec. For each photon spectrum, this fluence is given in Table 4. Had the results in Figure 9 been presented in the units of el/cm^2-sec-keV, all spectra would be identical above $\sim$1.7 keV with large differences below this energy. Instead,

TABLE 4. PHOTOEMISSION YIELD INFORMATION FOR THREE REPRESENTATIONS OF THE EWR SOURCE

The source is normally incident on Au.

	SOURCE			ELECTRON EMISSION			
SPECTRUM	*	ph/cm^2-sec	cal/cm^2-sec	el/cm^2-sec	el/ph	coul/cal	MEAN ENERGY
1	25%	0.66	5.45×10^{-17}	1.10×10^{-2}	1.66×10^{-2}	3.22×10^{-5}	1.34 keV
2	50%	0.98	7.47×10^{-17}	1.39×10^{-2}	1.54×10^{-2}	3.23×10^{-5}	1.44 keV
3	75%	1.93	1.35×10^{-16}	2.74×10^{-2}	1.42×10^{-2}	3.25×10^{-5}	1.53 keV

*Percent of total photon energy in the 1.6 keV feature.

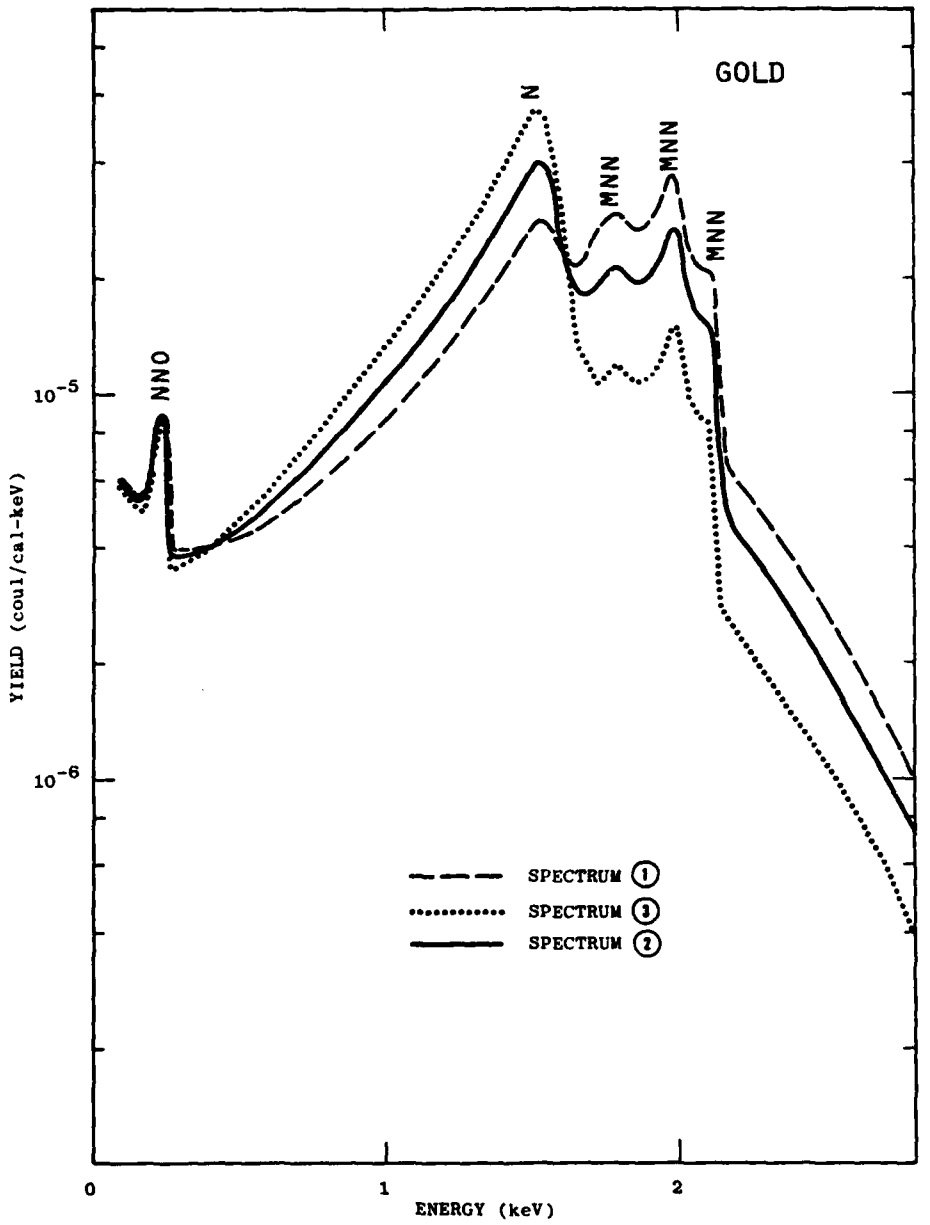

FIGURE 9. Calculated Photoemission Spectra for Three Representations of the EWR Photon Spectrum. The Representations are Specified in Section 2.3.

the spectra pivot with respect to one another about 1.7 keV due to the scaling by the different fluence values.

Although significant differences exist between the three photoemission spectra in Figure 9, all give essentially the same yield of 3.2×10^{-5} coul/cal, as shown in Table 4. This is due to the fortuitus circumstance that each component of the EWR spectrum, i.e., the 1.65 keV feature and the broader, more energetic continuum, give nearly the same yield in coul/cal. Thus, all mixtures of these components must give similar yields. This will not be the case for other materials. More yield variation between the components exists in units of el/ph which, in turn, leads to greater differences in this yield between the various EWR spectra, as shown in the table.

2.4 PHOTOEMISSION AND ELECTRON BACKSCATTER FROM Au FOR NARROW ENERGY SOURCES

SXRP photoemission spectra and yields will be presented in this section for narrow Gaussian photon distributions peaking at 1.0, 2.0, 2.5, and 5.0 keV. An electron backscattered spectrum and its total yield will also be presented for a 2 keV incident electron source. The above photon energies are in key regions with respect to the EWR spectrum and locations of photoabsorption edges. An incident electron energy of 2 keV is at a good value for testing the elastic scattering differential IMFP in the region pertinent to electron transport for an EWR source.

Table 3 gives the calculated and measured total yields for the above sources, as well as for the previously discussed EWR spectrum. The calculated photoemission yields for the Gaussian sources are also shown in Figure 10 which includes measured and empirically predicted yields from 0.1 to 10 keV. The data and the curve by Burke previously appeared in a paper by him.[26] The value of this figure is in showing the yield dependence as a function of hν. Thus, even though a data point does not exist to 2.5 keV, we can closely estimate what the value should be from the available data, as well as from the empirical curves which give a good indication of how the yield changes in the vicinity of the various edges. We see for the above sources, that good agreement is obtained with the measurements which suggests we have achieved a good representation of basic atomic model in terms of photoabsorption coefficients, the elastic DIMFP, the inelastic DIMFP's, and the Auger energies and yields. The agreement also suggests that we have obtained a good representation of the EWR photoemission spectrum and total yield for Au.

Figures 11-14 show the photoemission spectra and cumulative yields for the four Gaussian sources. The major contribution to photoemission for 1 and 2 keV photons on Au comes from N shell photoelectrons since these energies are below the energy of any of the M subshell edges. The results for the photon energies of 2.5 and 5.0 keV are significantly different, however, since there are now M edges below these energies. The dominant source of photoemission for 2.5 keV photons is Auger emission arising from the M_4NN and M_5NN Auger transitions. For 5.0 keV photons, the MNN Auger features still dominate although an important M photoelectron feature now appears at 2.8 keV.

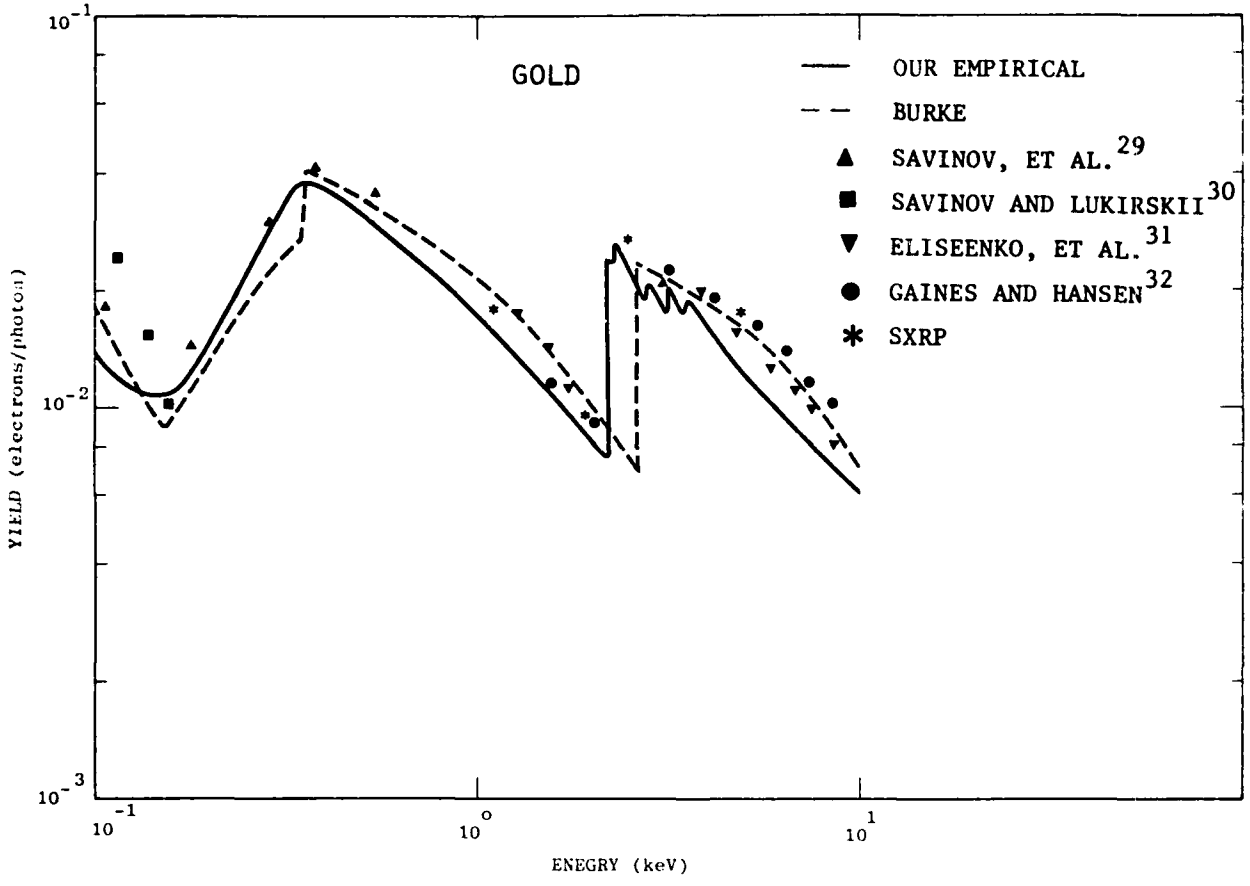

FIGURE 10. Photoemission Yield for Au versus hν from 0.1 to 10 keV. The Measured Values and the Dashed Curve Originally Appeared in a Paper by Burke.[26]

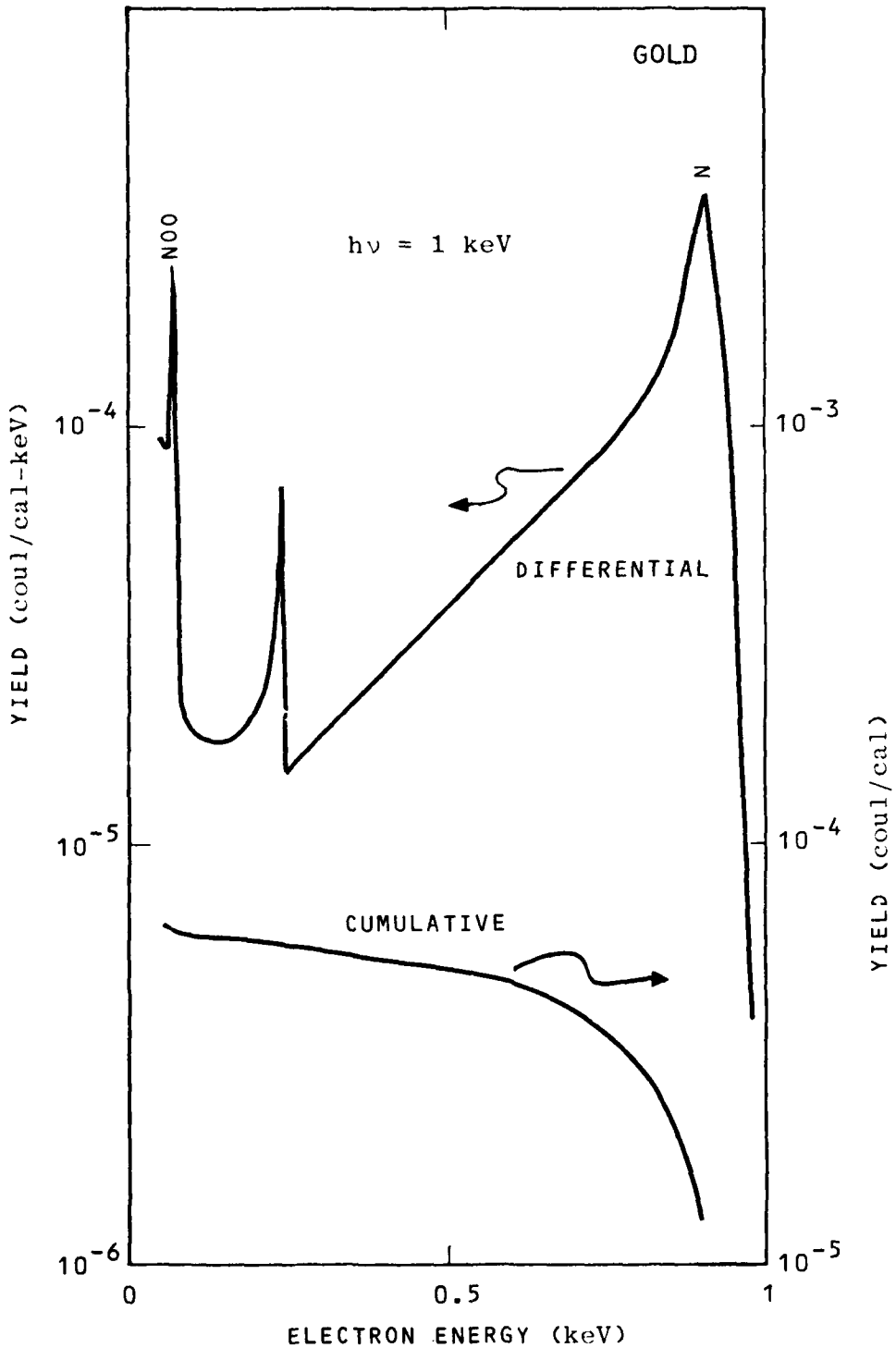

FIGURE 11. Calculated Photoemission Spectrum and Cumulative Back Yield for a Narrow 1 keV Gaussian Photon Source Incident on Au.

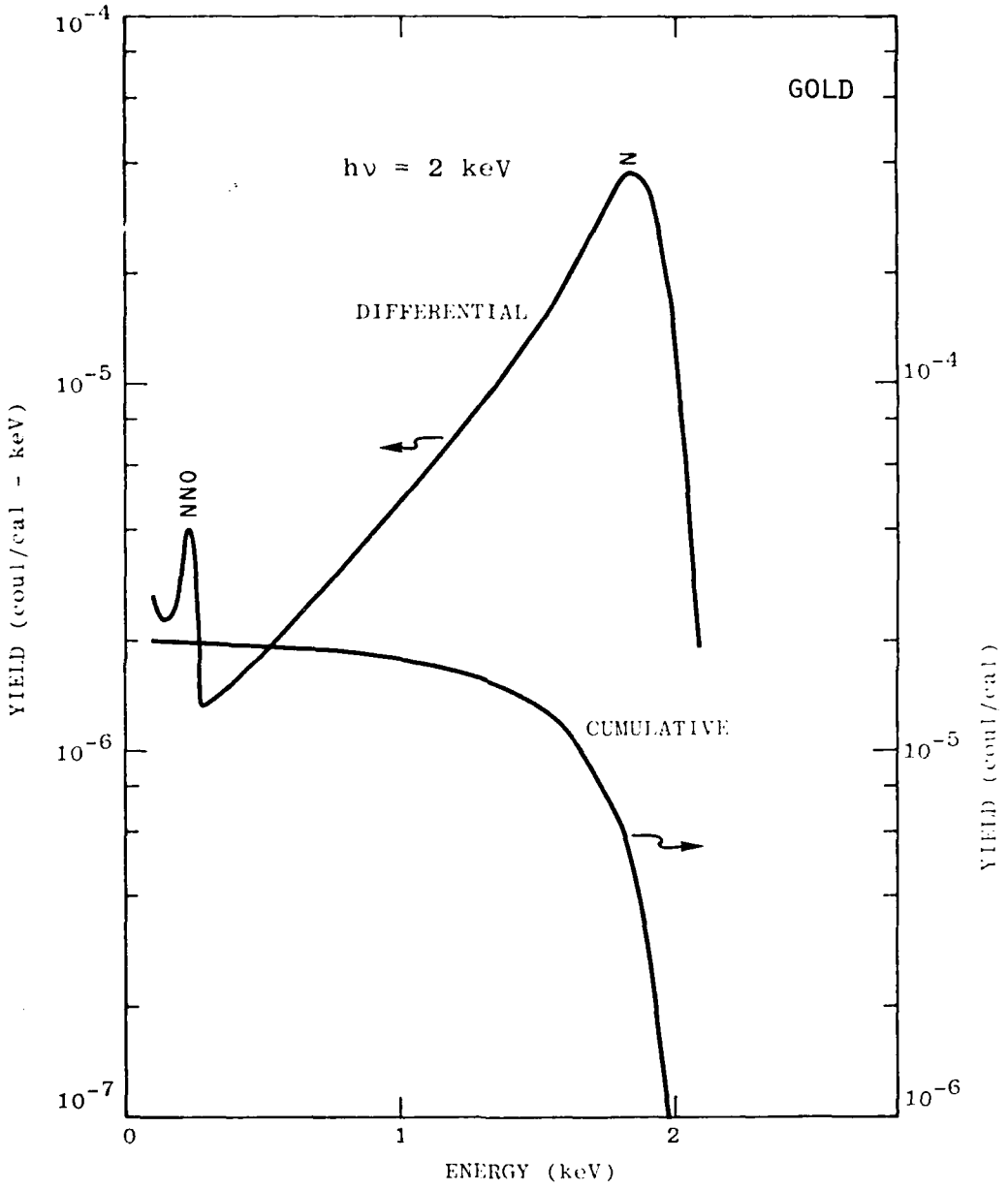

FIGURE 12. Calculated Photoemission Spectrum and Cumulative Back Yield for a Narrow 2 keV Gaussian Distribution Incident on Au.

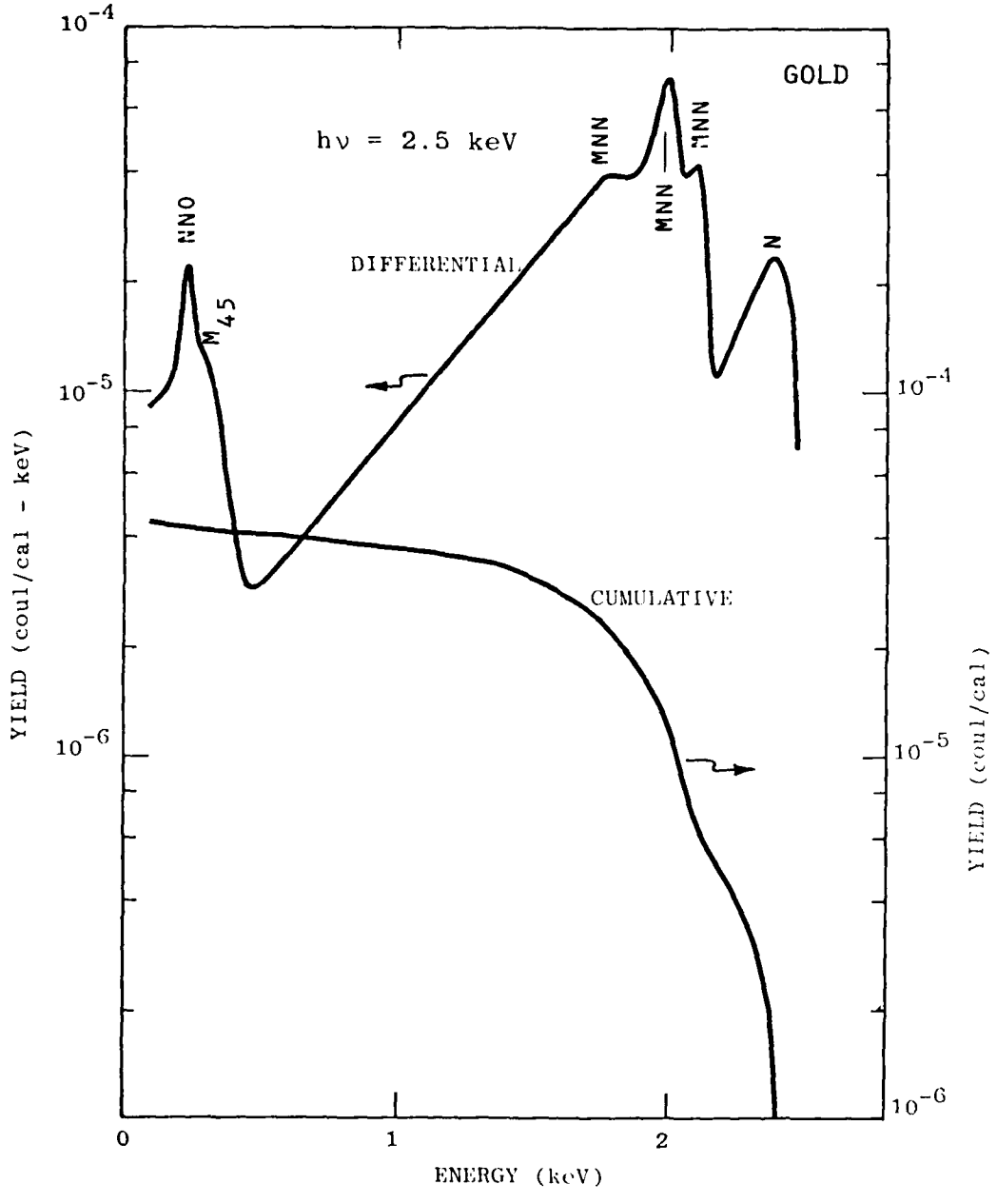

FIGURE 13. Calculated Photoemission Spectrum and Cumulative Back Yield for a Narrow 2.5 keV Gaussian Distribution Incident on Au.

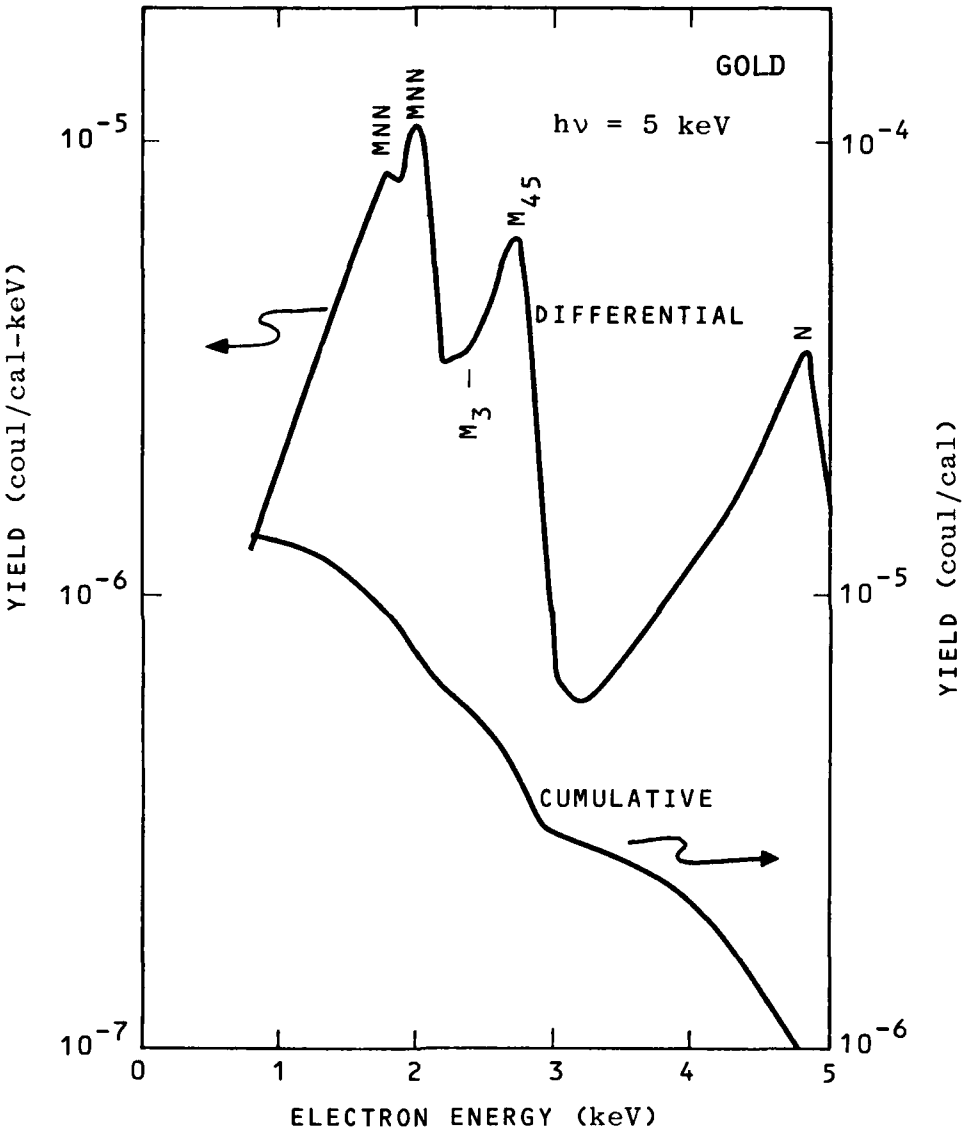

FIGURE 14. Calculated Photoemission Spectrum and Cumulative Back Yield for a Narrow 5 keV Gaussian Photon Source Incident on Au.

Figure 15 shows the backscattered spectrum and cumulative yield for a 2 keV Gaussian electron source incident on Au. The incident spectrum, given by the dashed curve is also shown. The incident electrons are not all normally incident, but rather have the Gaussian distribution shown in Figure 16 as a function of μ, the cosine of the angle of incidence. Included in the figure is the approximate variation of the backscatter yield for Au as a function of μ.[28] Based on Figure 16, the yield obtained with the given angular dependence of the incident electrons must be reduced by 0.93 to compare with data taken for normally incident electrons. The calculated value appearing in Table 3, 53%, has been adjusted to normal incidence by the above factor from the value 57% appearing in Figure 15. From the table, it is seen that good agreement is achieved between the calculations (53%) and measurements (50%).[28]

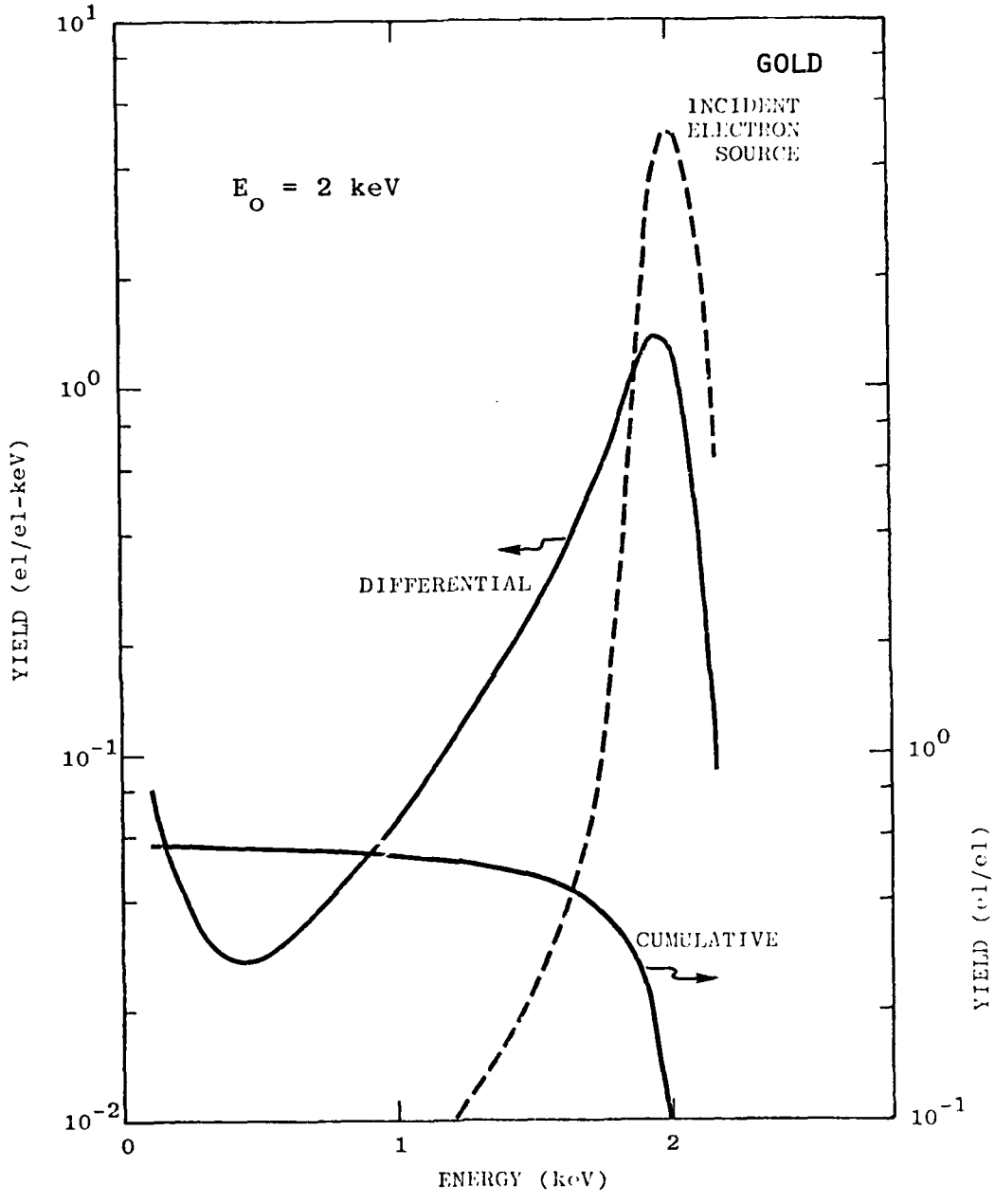

FIGURE 15. Calculated Electron Backscattered Spectrum and Cumulative Back Yield for the Shown 2 keV Gaussian Distribution Incident on Au.

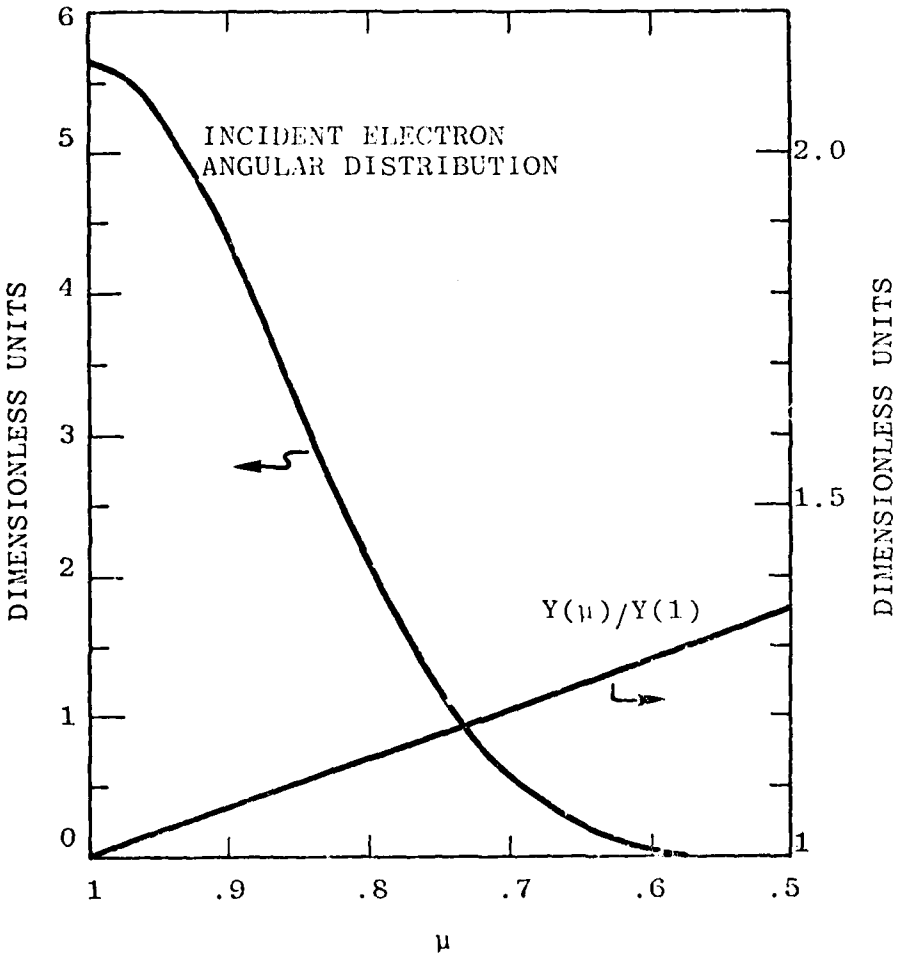

FIGURE 16. Gaussian Angular Distribution of the 2 keV Incident Electron Flux and the approximate Total Backscatter Yield. μ is the Cosine of the Angle of Incidence.

Section 3

THE REMAINING MATERIALS SILVER, COPPER AND CARBON

In this section, material models and photoemission results for the EWR source will be presented for the remaining three materials — silver, copper, and carbon. Furthermore, comparisons with EWR photoemission data will be made where possible, namely, for silver and copper.

3.1 SILVER

Silver represents a conductor of intermediate atomic number (Z=47). Its density is 10.5 g/cm^3. The 47 electrons are distributed among the shells K through O. Similar to Au, we have lumped together various subshells whose binding energies are close together. Table 5 gives our representation of the shell structure together with binding energies.[15] The electrons within the specified shells are treated as inner shell electrons and are thus given an atomic description in terms of specifying IMFP's. The O shell is not included in Table 5 since its single electron has been assigned to the conduction band and is thus given a solid-state description in terms of IMFP specifications. The Fermi energy E_F used to specify the conduction band and plasmon IMFP's is taken to be 5.5 eV which comes from Kittel[33] and which is also consistent with the assignment of one electron/atom to the conduction band.

TABLE 5. BINDING ENERGIES OF Ag

SHELLS	BINDING ENERGY (keV)
K	24.7
L	3.35
M_1	0.665
M_{23}	0.567
M_{45}	0.384
N	0.0127

Our Auger spectroscopy is given in Table 6 and similar to Au, is based on lumping together various Auger features but in such a way as not to exclude important contributions to the process of photoemission. Handbook of Auger Electron Spectroscopy[24] and Storm and Israel's Report[15] were used to specify the averaged features and yields. Unlike our spectroscopy for Au, we consider only a single MNN Auger feature for Ag. This is due to the smaller Auger energies for Ag and, in turn, the smaller energy differences between the various features.

For the shell representation in Table 5, the photoabsorption coefficients are shown in Figure 17. The technique for specifying individual shell contributions is the same used for Au. The sum of coefficients (solid line) and data points come from Hubbell.[14]

The inner shell IMFP's for shells M_1-N are shown in Figure 18. Similar to Au, they are based on our technique originally discussed in a recent report[6] and since then in more detail in an IEEE publication.[8] The basis for a given IMFP is the corresponding photoabsorption coefficient. From a practical standpoint, the M_1 and M_{23} IMFP's could be eliminated from our transport description and for most applications, M_{45} as well.

The conduction band and plasmon IMFP's are shown in Figure 19, together with the sum of inner shell IMFP's and the sum of all inelastic IMFP's. The ORNL free electron gas model[22] was used to specify the conduction band and plasmon IMFP's as was done for Au. The applied Fermi energy was 5.5 eV, as noted above. We see, in our description, that the dominant contribution to the total inelastic IMFP comes from N shell electrons.

TABLE 6. AUGER FEATURES OF Ag

TRANSITION	ENERGY (keV)	YIELD
KLL	18.8	0.166
LMM	2.57	0.900
MNN	0.355	1.000

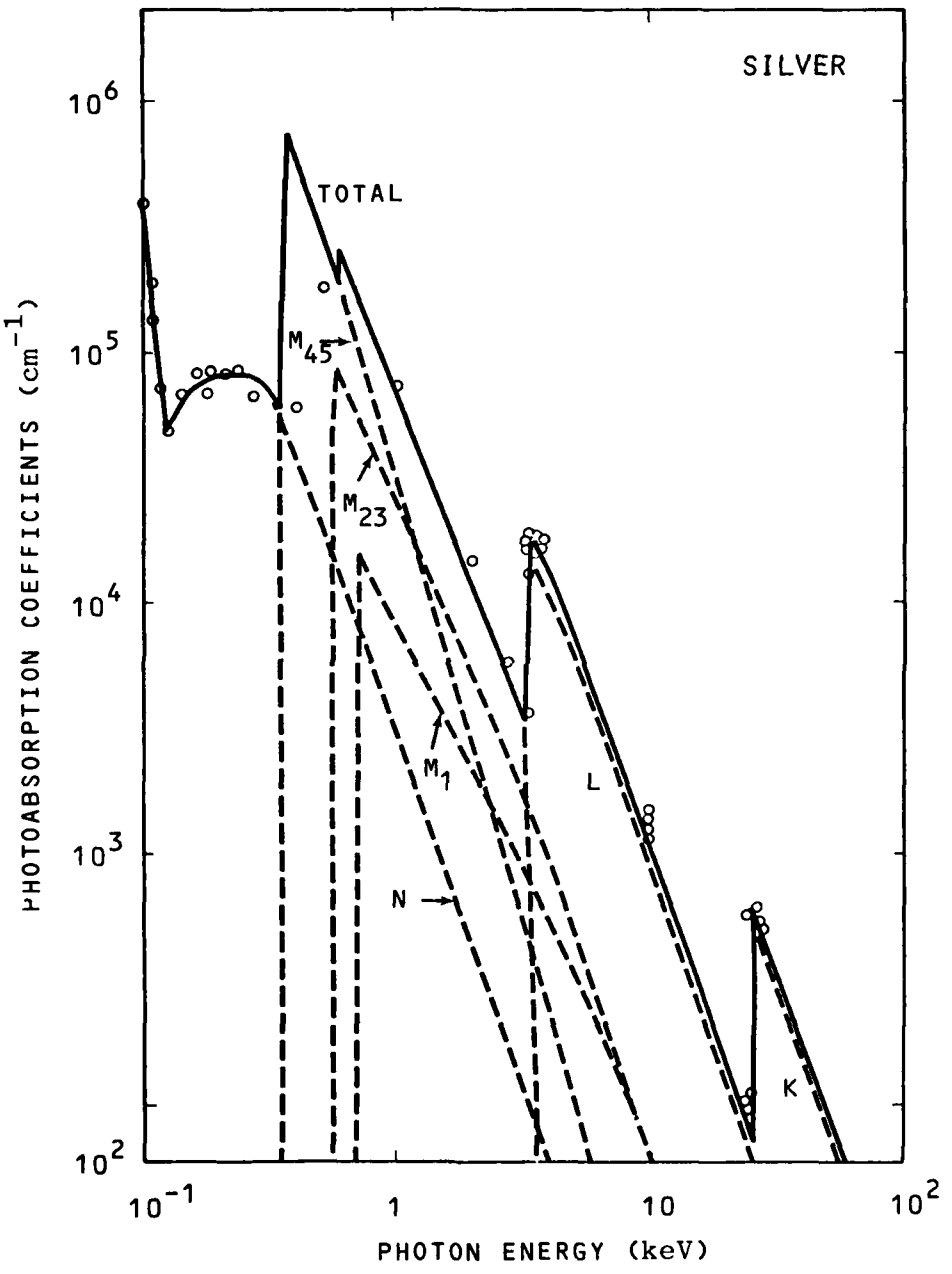

FIGURE 17. Photoabsorption Coefficients for Ag.

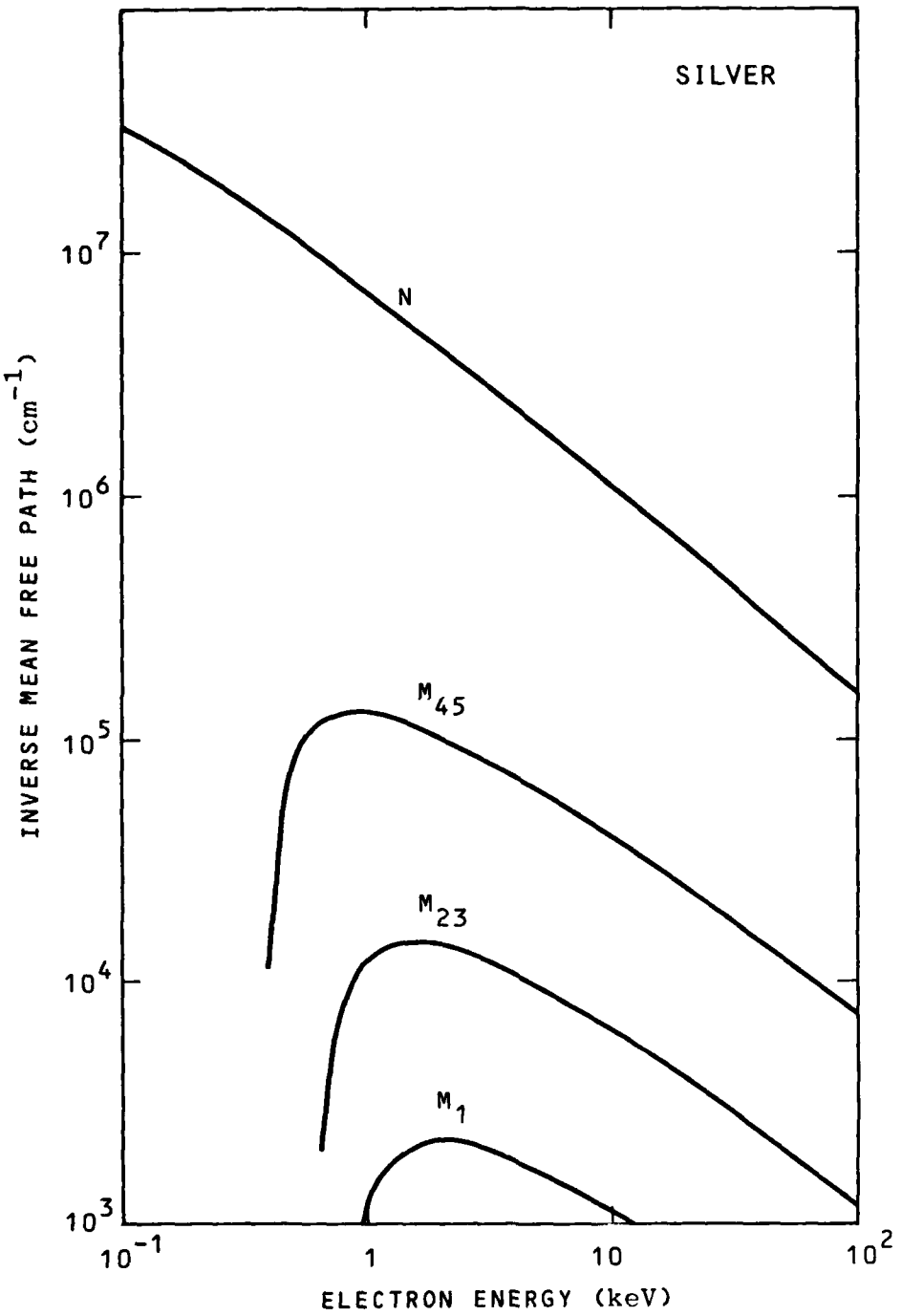

FIGURE 18. Inner Shell Inverse Mean Paths of Ag.

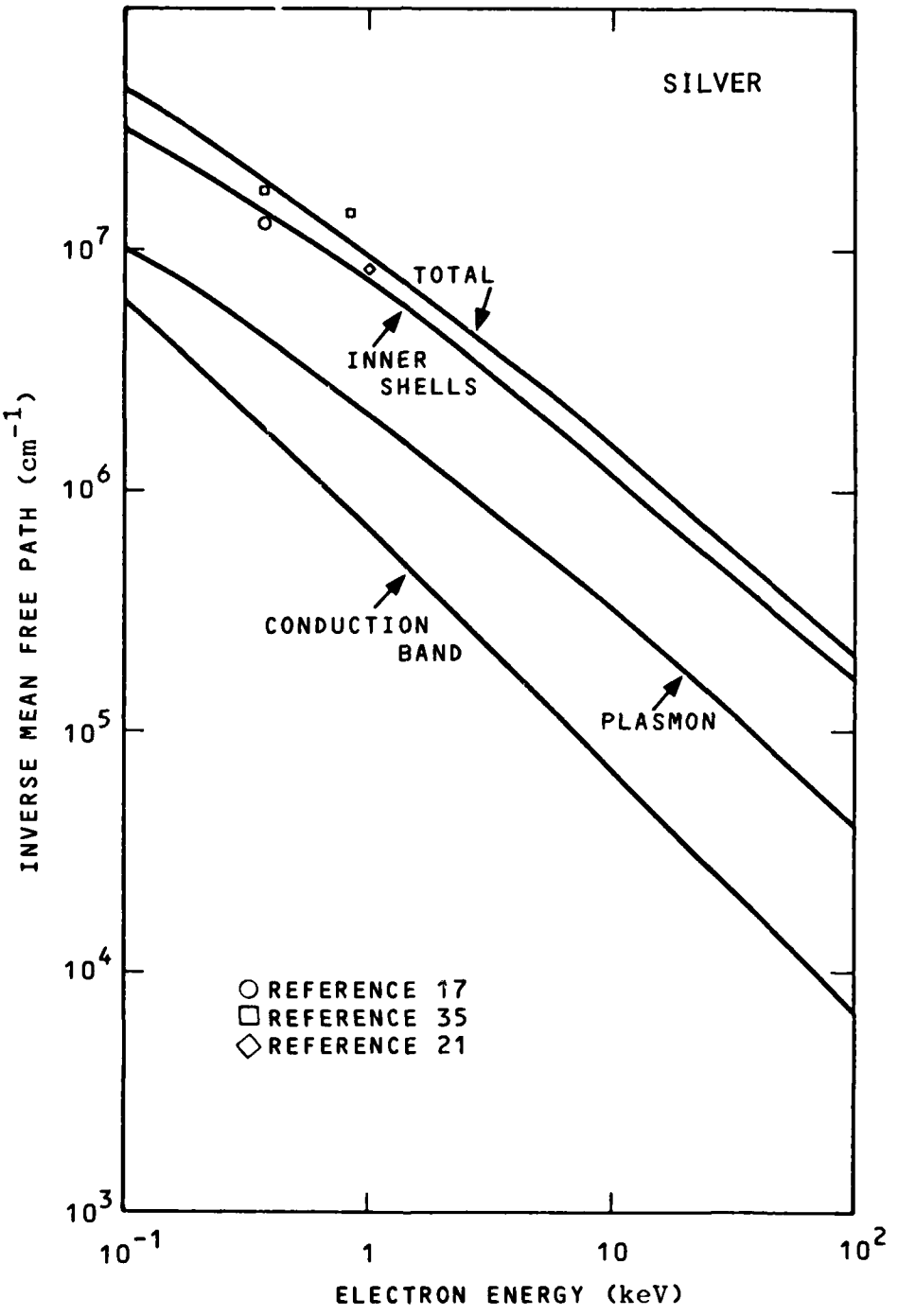

FIGURE 19. Inelastic Inverse Mean Free Paths of Ag.

The elastic IMFP is shown in Figure 20, together with the total inelastic IMFP from the previous figure. We used the same description here used previously for Au with Z=79 replaced by Z=47. Elastic scattering is less important for Ag than for Au as can be seen by comparing Figures 3 and 20.

Various stopping powers are shown in Figure 21, including one by the ORNL group based on a statistical model.[34] Good agreement is obtained, except at low energies. We anticipate that our total value is somewhat too high at low energies due to the first Born approximation becoming less valid.

The calculated photoemission spectrum for the EWR source shown in Figure 4 incident on Ag is shown in Figure 22. The spectrum is dominated by M photoelectron contributions. The integrated yield down to ~0.1 keV is 8.9×10^{-6} coul/cal. The spectrum and yield may be compared with data by Bernstein[10] and Fromme, et al.[11] in Figure 23. Reasonably good agreement in shape is obtained with Bernstein's spectrometer data although his yield is approximately twice as high. The source of this difference has not yet been determined, but will be investigated within the next few months.

A comparison of photoemission properties of Ag with the previously investigated materials Aℓ and Au is worth noting. Compare, e.g., Figure 22 with Figure 7. We see that all three spectra are distinctly different from one another. The spectrum of Ag, e.g., is noticeably softer than that of Au and possesses a yield about one-third as large. It should be noted, however, as has been done before, that such relative behavior is strongly dependent on the photon source spectrum.

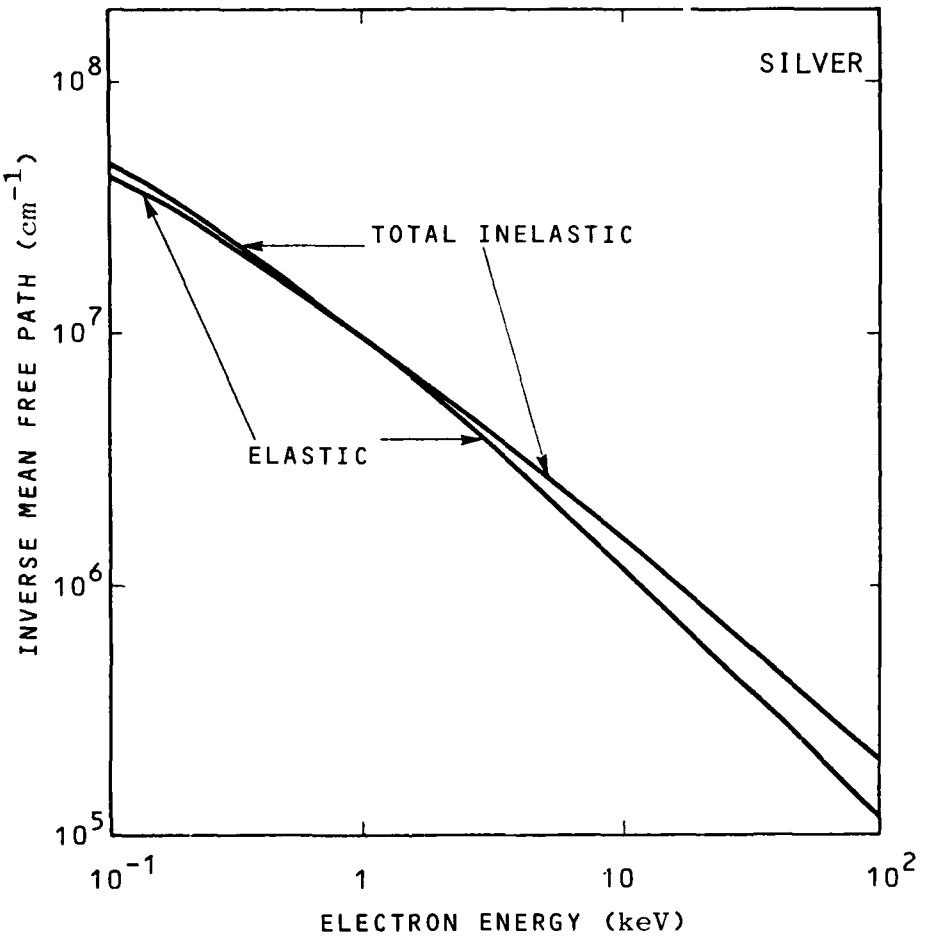

FIGURE 20. Total Inelastic and Elastic Inverse Mean Free Paths of Ag.

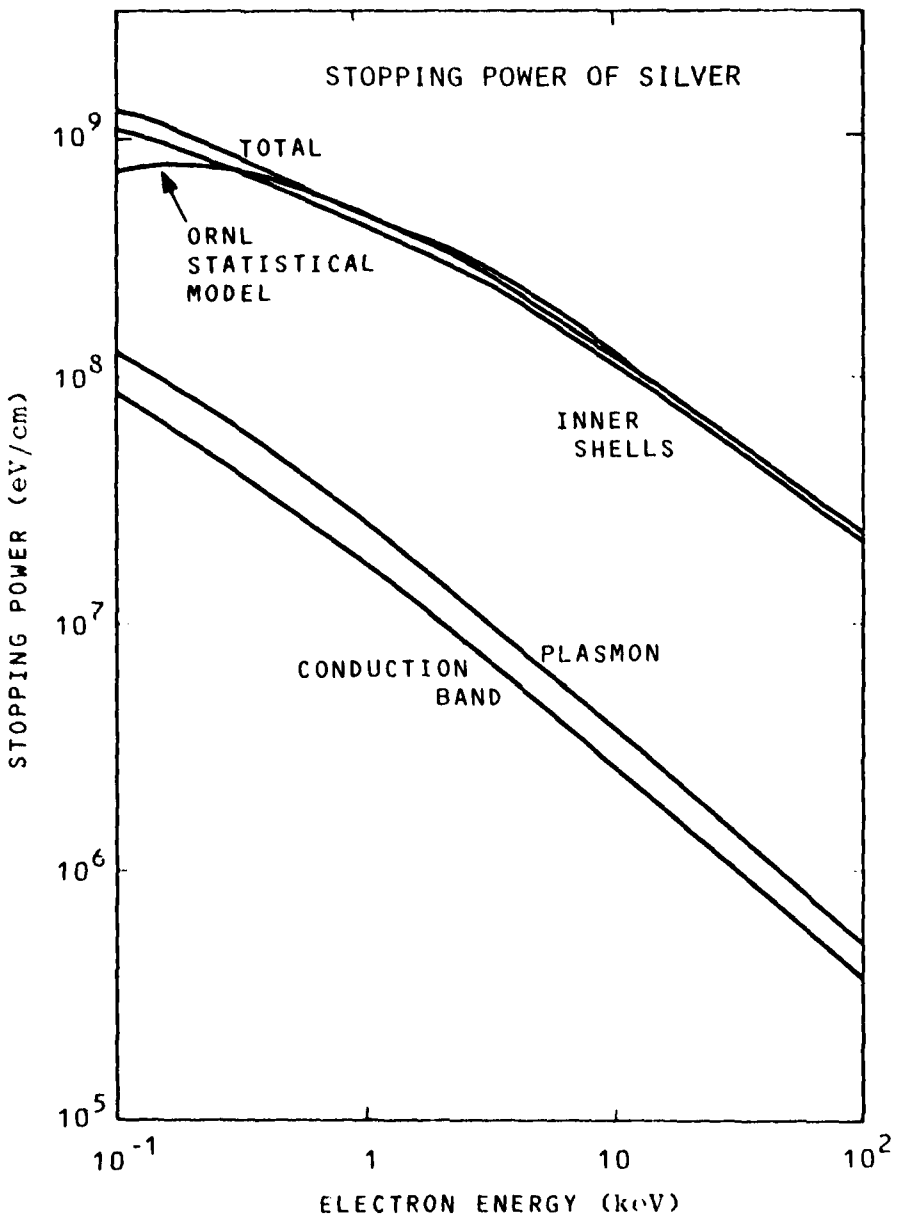

FIGURE 21. Individual Stopping Powers of Ag. ORNL curve is from Reference 34.

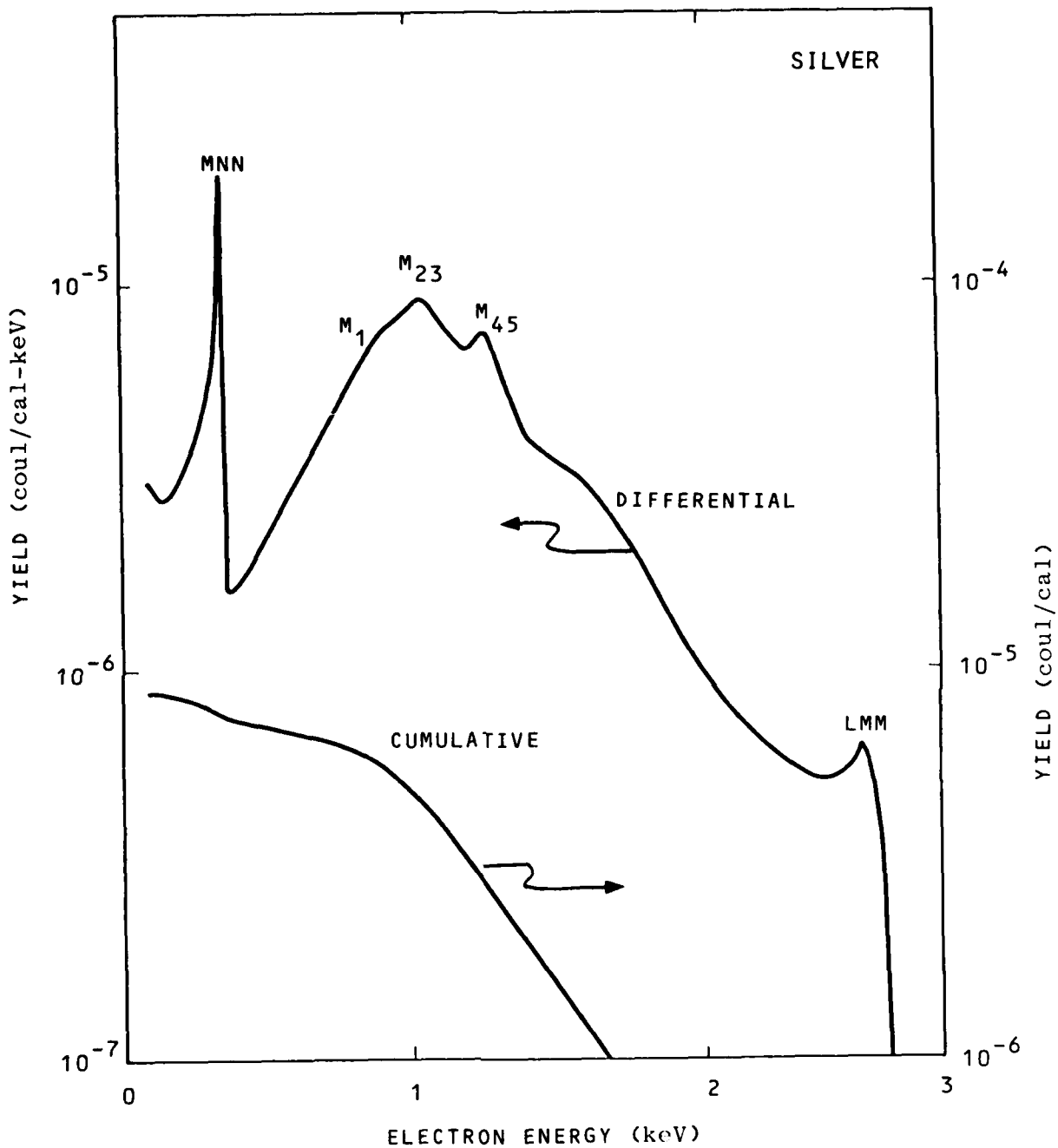

FIGURE 22. Calculated Photoemission Spectrum and Its Cumulative Back Yield for an EWR Source Incident on Ag.

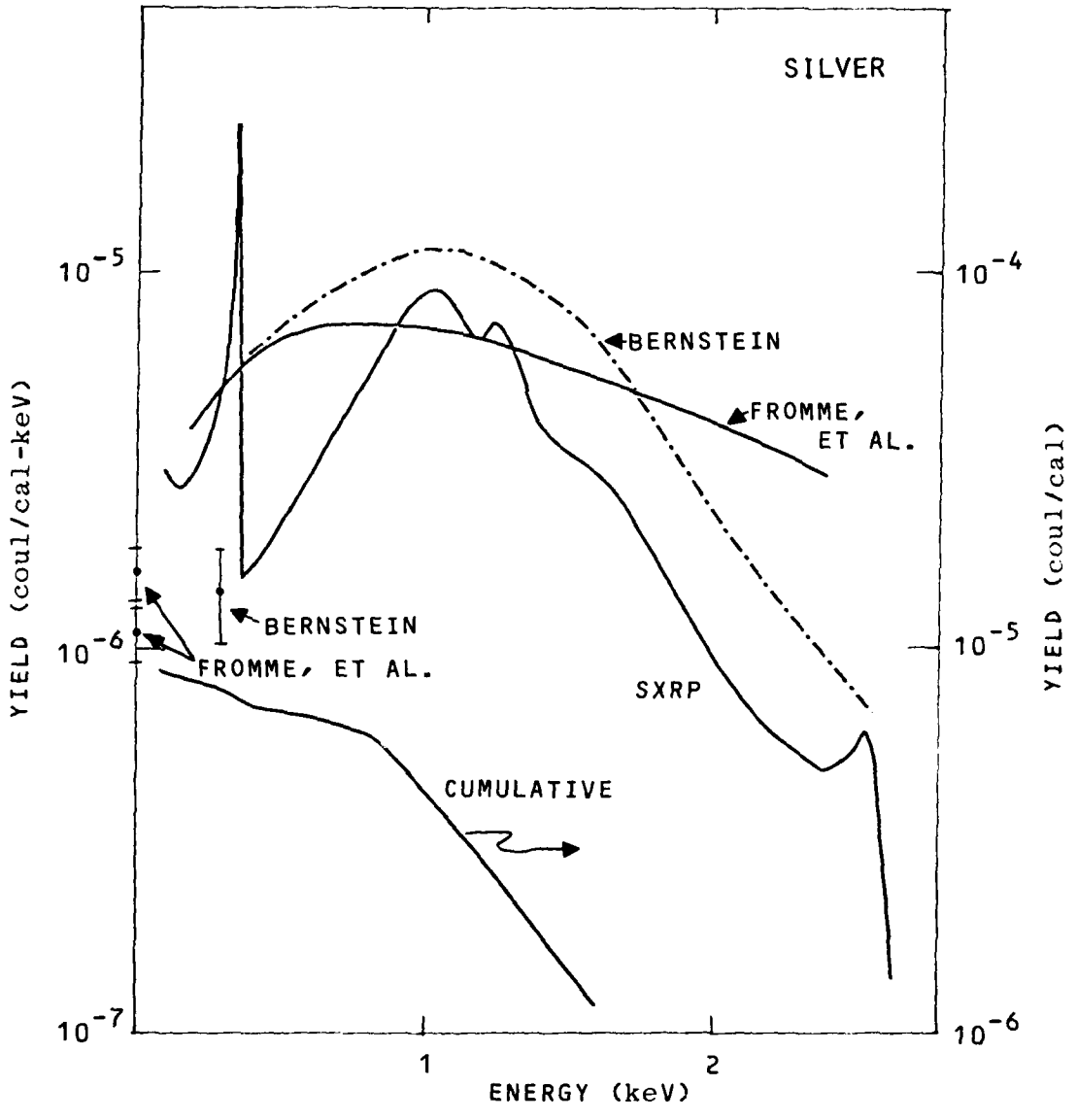

FIGURE 23. Calculated and Measured Photoemission Spectrum and Cumulative Back Yield for an EWR Source Incident on Ag.

3.2 COPPER

Copper is the sixth material to be investigated in our program of soft x-ray photoemission. The previous five, as well as the last material discussed in this report (Carbon), were selected for the primary purpose of complimenting experimental efforts in the SKYNET program. Photoemission measurements have not, however, been made for Cu as of this time. Our reasons for including it in this original group of seven materials are that it is a commonly used conducting material and has a desirable atomic number (Z=27) in relation to the other materials. One of the goals of our overall program is to provide a data base spanning a wide range of Z-values with the Z-values of the selected materials somewhat uniformly distributed. Copper nicely "bridges the gap" between Aℓ (Z=13) and Ag (Z=47).

The description to follow of the material model of Cu will be brief since the applied techniques are those already used and described for Au and Ag. To begin with, Cu has a material density of 8.96 g/cm^3. The most loosely bound electron is an N or 4s electron which we have assigned to the conduction band. The corresponding Fermi energy E_F is 7 eV.[33] The remaining electrons are distributed among the K, L, and M shells with the binding energies shown in Table 7.[15] The required Auger description is particularly simple and is given in Table 8.[15,24] Only LMM Auger electrons are relevant to the work reported here.

The photoabsorption coefficients appear in Figure 24 based on total values tabulated by Hubbell.[14] The inner shell ionization IMFP's for shells L and M are shown in Figure 25. The L-shell IMFP is small enough that it will have little effect on the transport results.

TABLE 7. BINDING ENERGIES OF Cu

SHELL	BINDING ENERGIES (keV)
K	8.98
L	0.953
M	0.013

TABLE 8. AUGER FEATURES OF Cu

TRANSITION	ENERGY (keV)	YIELD
KLL	6.93	0.56
LMM	0.92	1.00

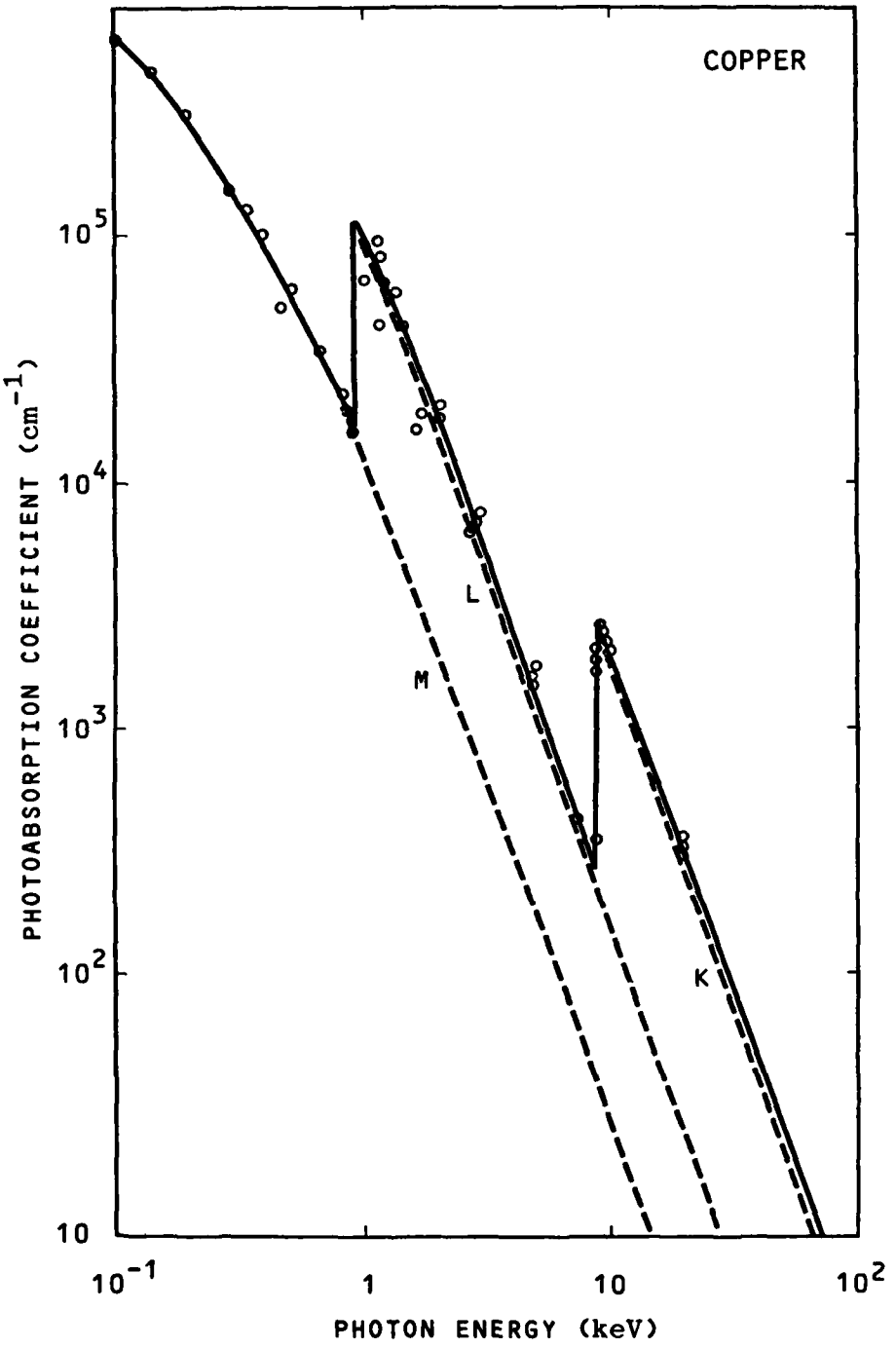

FIGURE 24. Photoabsorption Coefficients for Cu.

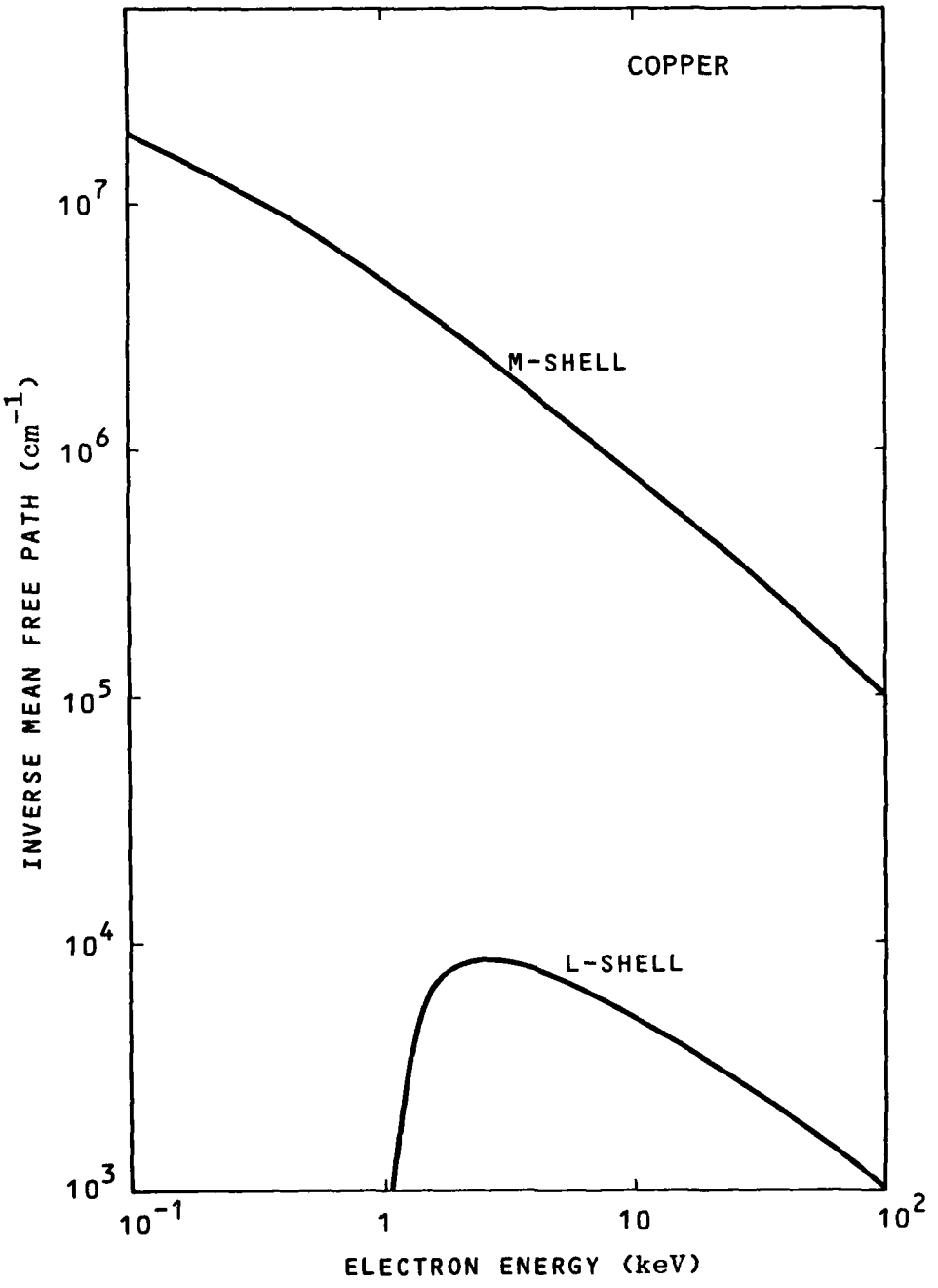

FIGURE 25. Inner Shell Inverse Mean Free Paths for Cu.

The total inelastic IMFP, together with its components and available measured values, are shown in Figure 26. The M-shell IMFP is seen to dominate the total based on assigning 1 e/atom to the conduction band. The total inelastic IMFP again appears in Figure 27, this time with the elastic IMFP. Similar to Ag, the two quantities are comparable to one another.

Stopping powers appear in Figure 28 based on the IMFP's just presented. Also shown is the stopping power by a statistical model calculated by Ashley, et al.[34] The statistical model does not assume the same shell structure used in this work. Instead, a mean inter-electron spacing r_s is used which is related to the Fermi energy by $E_F = (e^2/2a_o(9\pi/4)^{2/3}\ r_s^{-2}$, where a_o is the Bohr radius.

The calculated EWR photoemission spectrum for Cu appears in Figure 29. As noted above, measurements are not available to compare with this result. The given spectrum provides another example of how different photoemission properties can be from one material to the next (compare Figure 29 to Figures 7 and 23). This spectrum, e.g., is much softer than that for Au. Here, emission is dominated by L-photoelectrons and LMM Auger electrons below 1 keV.

3.3 CARBON

Carbon provides the basis for a number of insulating materials used on satellites, such as paint coatings and the dielectrics Kapton and Mylar. Thus, modeling and investigating photoemission characteristics of C in its pure form provides a reasonable starting point

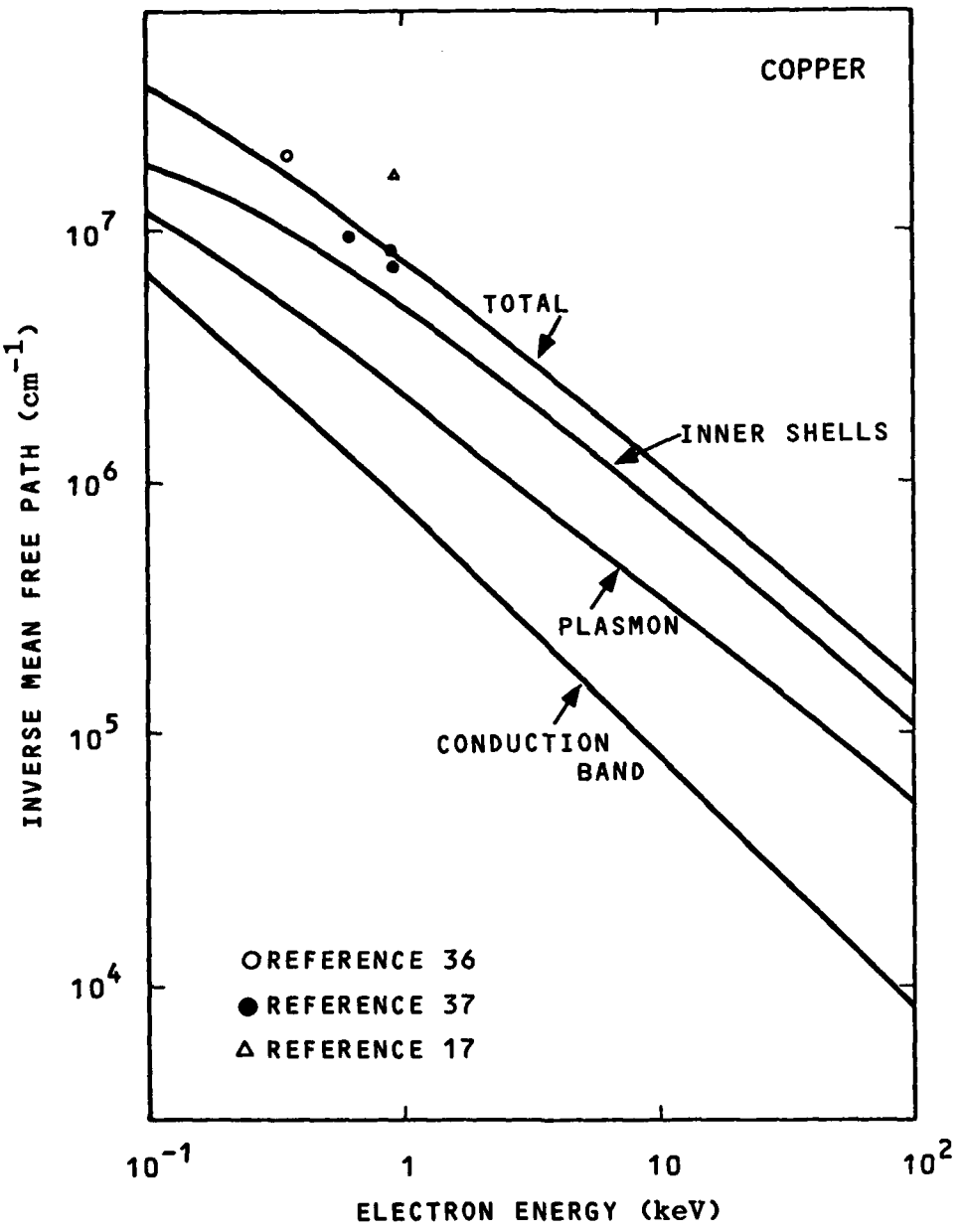

FIGURE 26. Inelastic Mean Free Paths of Cu.

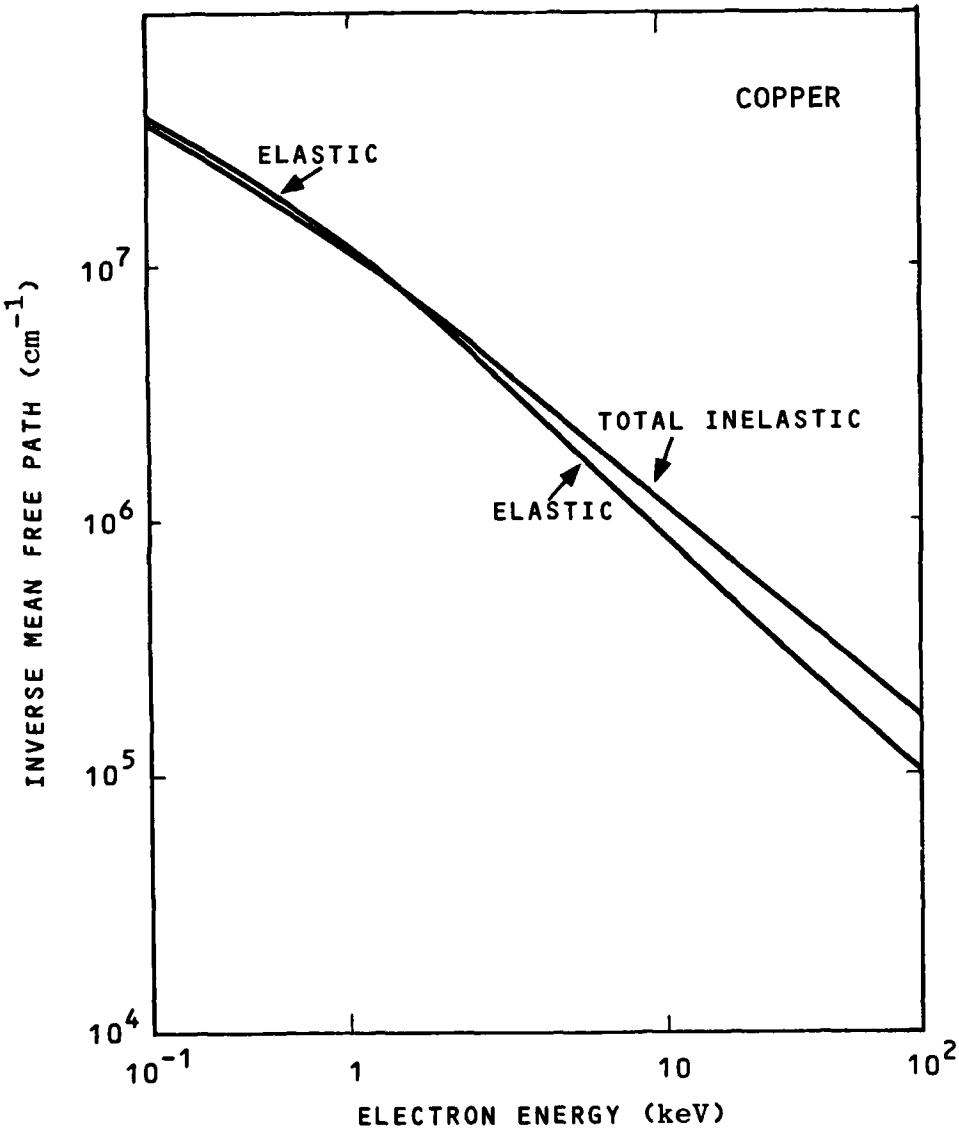

FIGURE 27. Total Inelastic and Elastic Inverse Mean Free Paths of Cu.

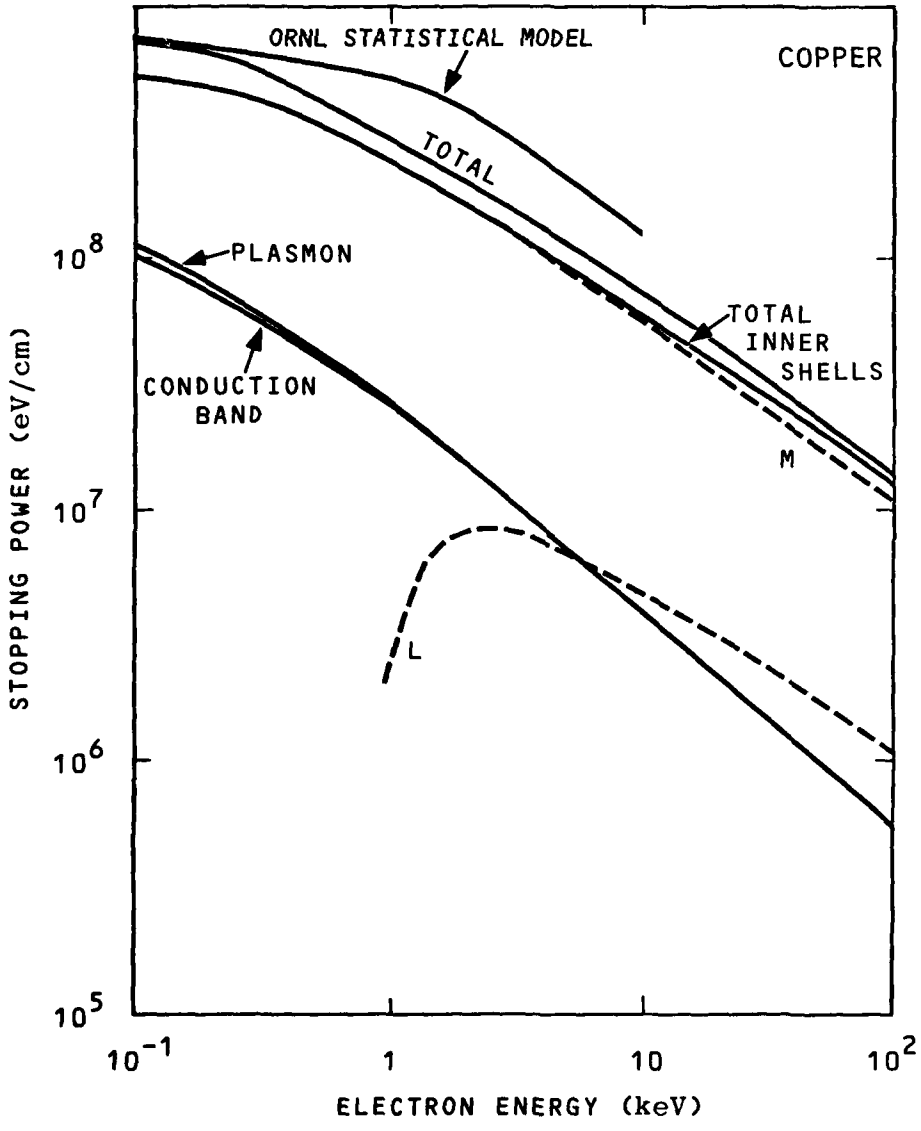

FIGURE 28. Stopping Power of Cu due to Conduction Band Electrons, Plasmon Excitation, and Inner Shell Electrons.

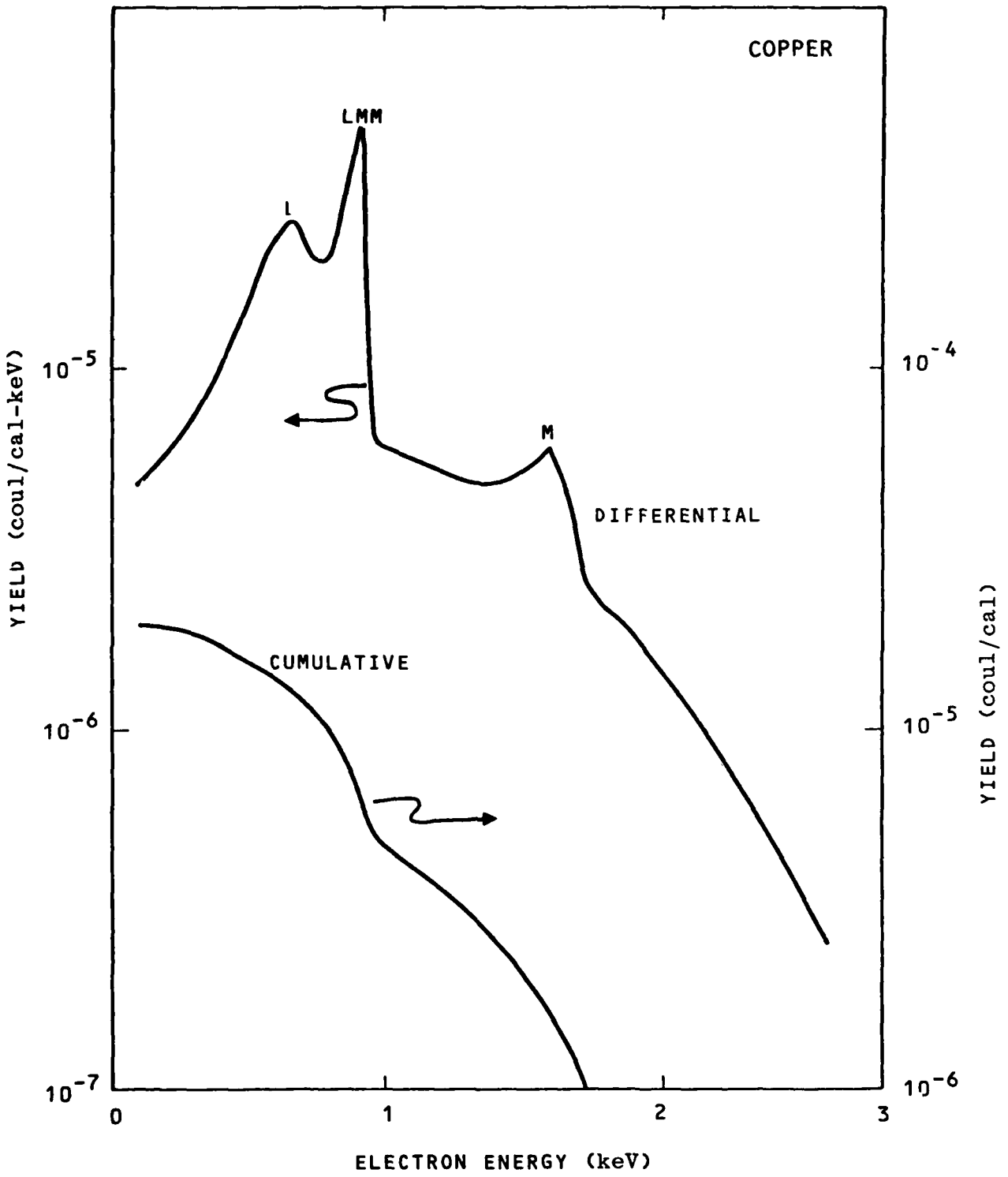

FIGURE 29. Calculated Photoemission Spectrum and Its Cumulative Back Yield for an EWR Source Incident on Cu.

for investigating these more complicated materials. The density chosen for C in this work is 2.25 g/cm^3, the density of graphite. Carbon has a Z-value of only 6 with two electrons in the K-shell and the remaining four in the L-shell. The binding energies for these shells are given in Table 9. The single Auger feature, that for a KLL transition, appears at 0.272 keV with a yield of unity (Table 10).

The photoabsorption coefficients are shown in Figure 30, based on the Hubbell tabulations.[14] The corresponding inner shell ionization IMFP's are shown in Figure 31, together with a result by Ashley, et al.[38] for polystyrene based on their insulator model. The ORNL result has been scaled by the ratio of densities of graphite and polystyrene. If the agreement shown is not simply fortuitus, it indicates that a pure atomic description is adequate for C.

The total inelastic IMFP (essentially the L-shell IMFP) is shown, together with the elastic IMFP in Figure 32. As expected, the inelastic component dominates due to the low Z nature of C.

The stopping powers for K and L shells, together with that for polystyrene by Ashley, et al. appear in Figure 33. Again, the polystyrene value has been scaled as was done for the IMFP in Figure 31. The agreement is less satisfactory here than for the IMFP's. The problems may arise from the scaling procedure which was based on polystyrene being dominated in weight by C. Its chemical composition is given by C_8H_8. Hydrogen, undoubtedly, will produce different degrees of effect on the stopping power versus the total IMFP.

TABLE 9. BINDING ENERGIES OF C

SHELL	BINDING ENERGIES (keV)
K	0.284
L	0.008

TABLE 10. AUGER FEATURES OF C

TRANSITION	ENERGY (keV)	YIELD
KLL	0.272	1.00

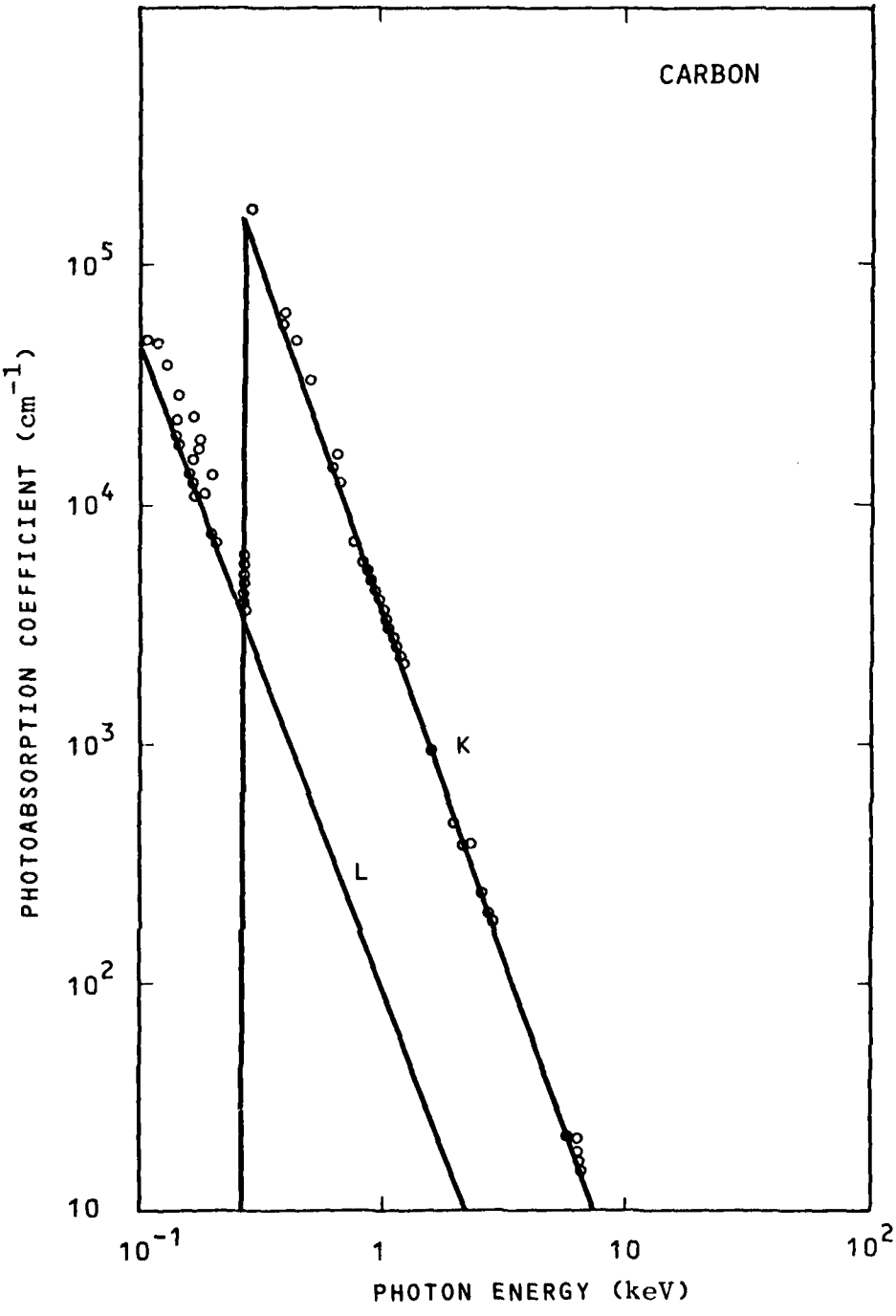

FIGURE 30. Photoabsorption Coefficients for C.

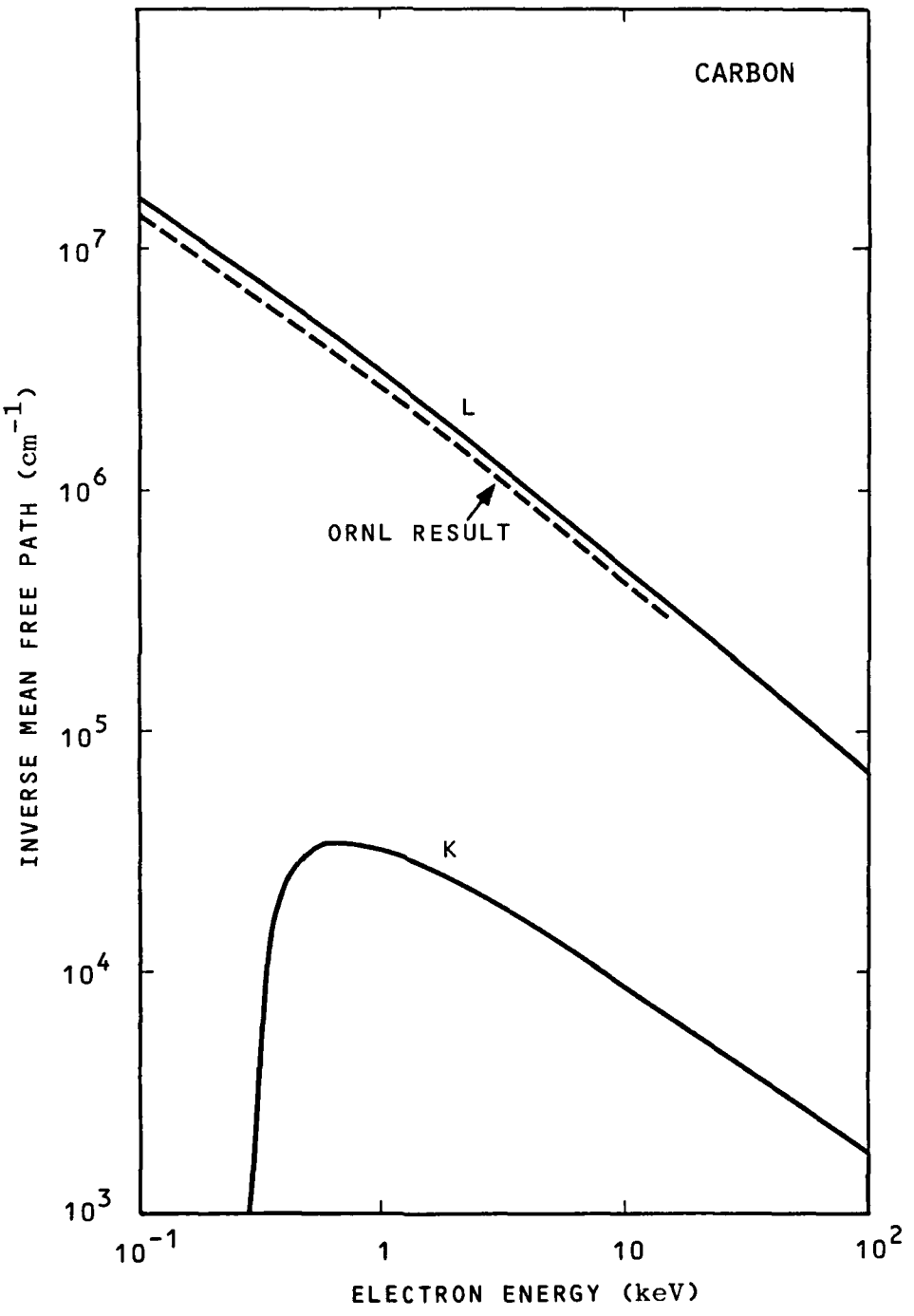

FIGURE 31. Inner Shell Inverse Mean Free Paths of C.

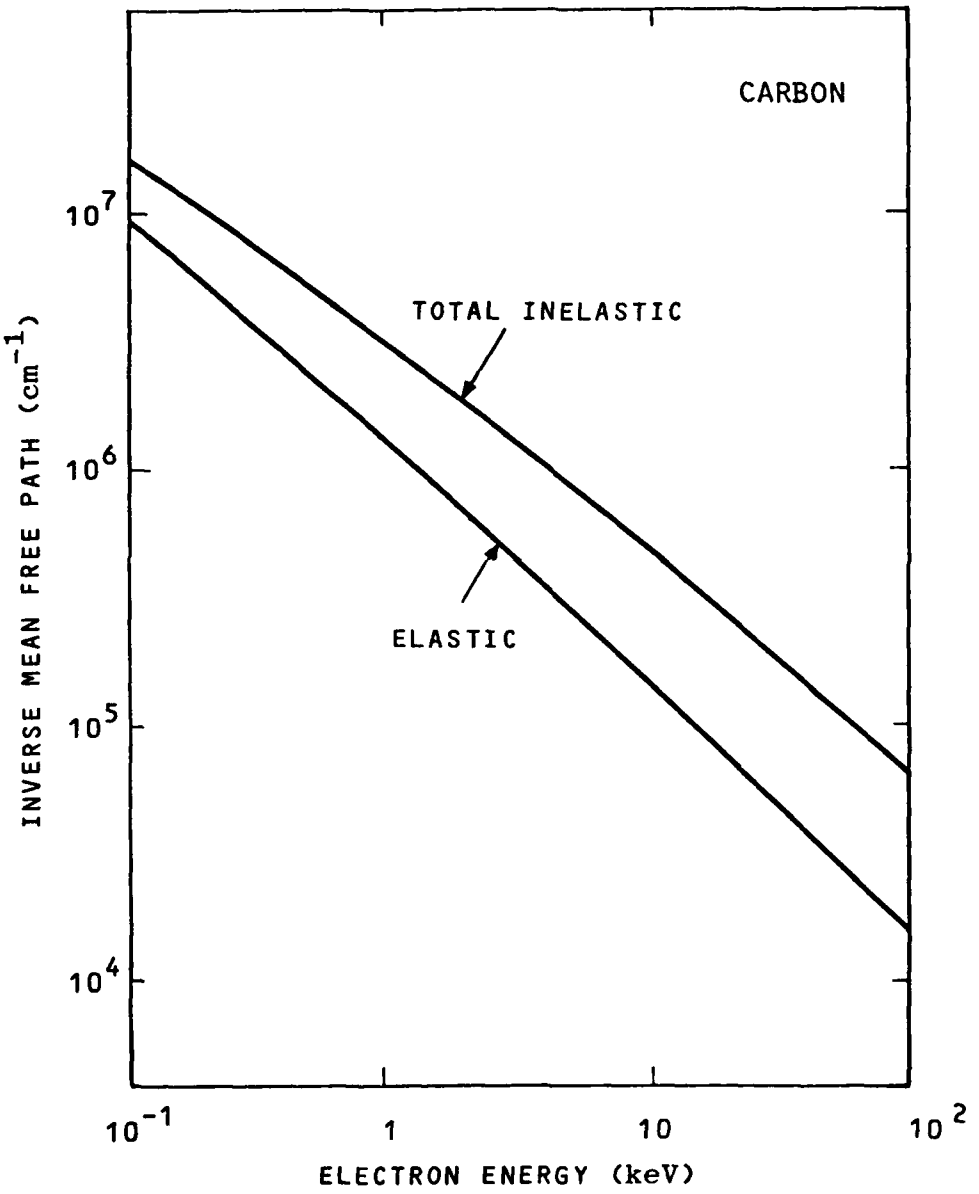

FIGURE 32. Total Inelastic and Elastic Inverse Mean Free Paths of C.

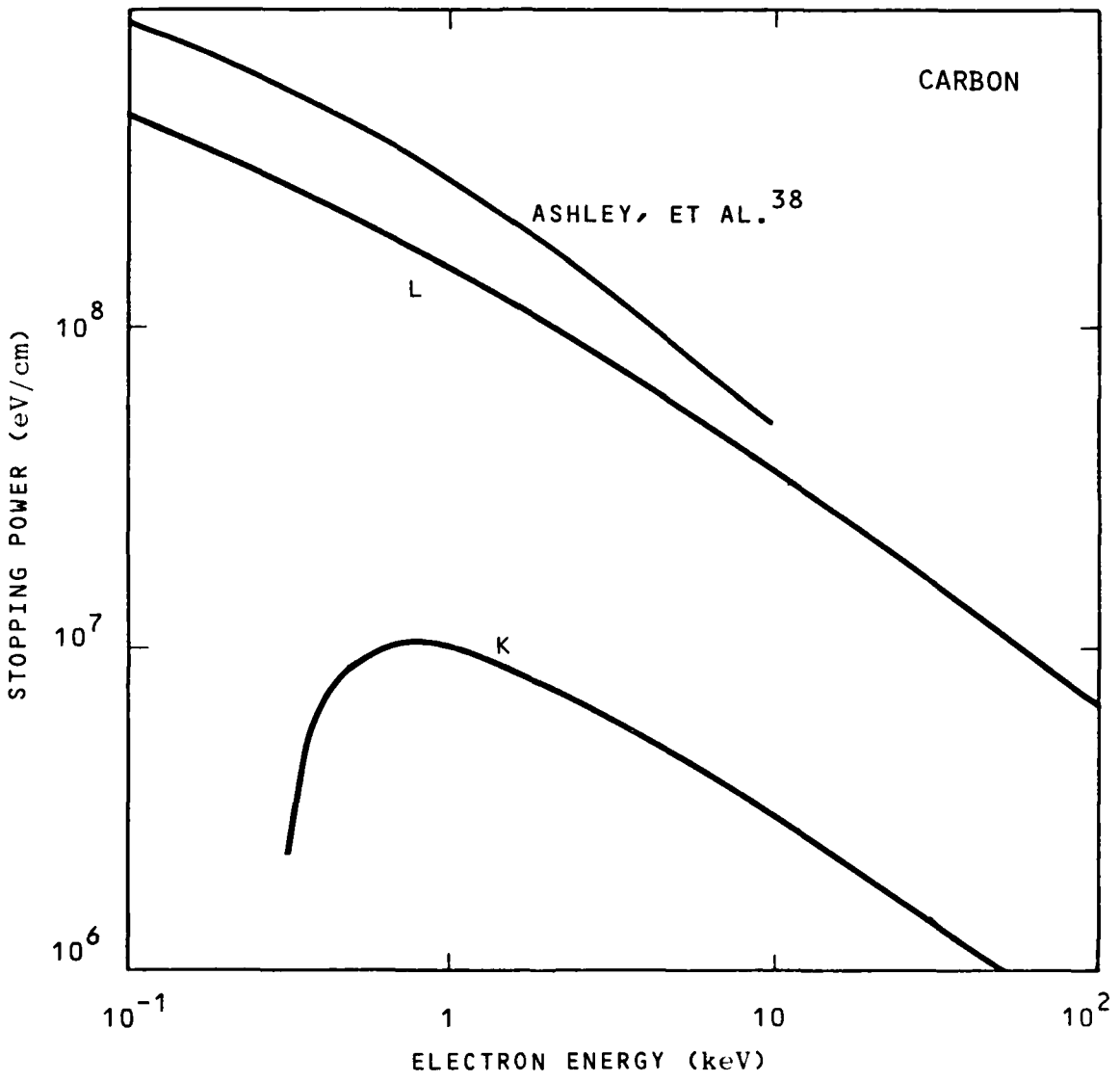

FIGURE 33. Stopping Powers of K and L Shell Electrons of C.

The EWR photoemission spectrum, together with its cumulative yield, are shown in Figure 34. They may be compared with measured values in Figure 35. Overall, good agreement is obtained between the calculations and the spectrometer data by Bernstein.

In conclusion, the calculated and measured yields for the EWR source incident on the various materials are given in Table 11. Carbon and gold possess the lowest and highest yields differing with each other by a factor of $\sim$15.

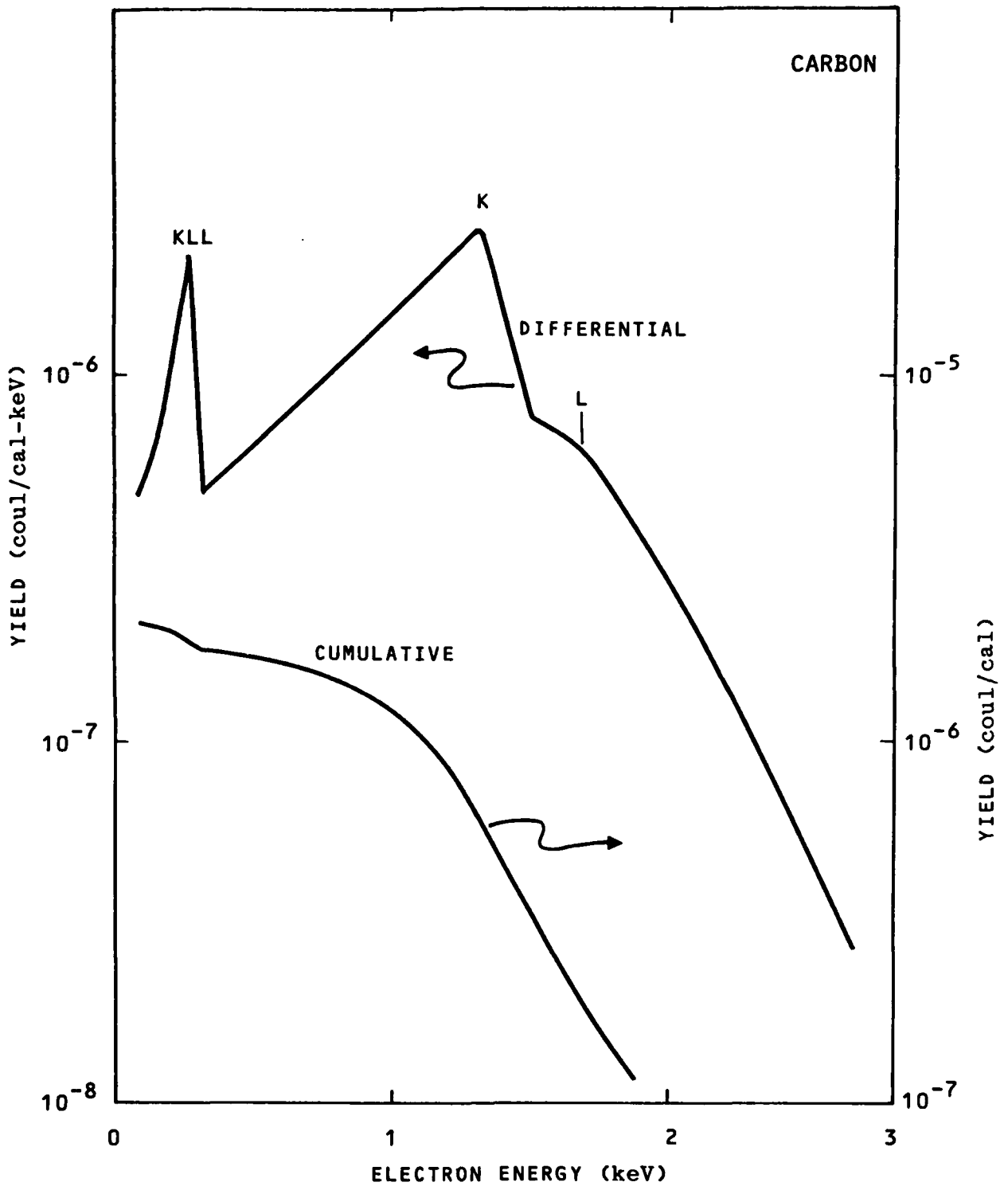

FIGURE 34. Calculated Photoemission Spectrum and Its Cumulative Back Yield for an EWR Source Incident on C.

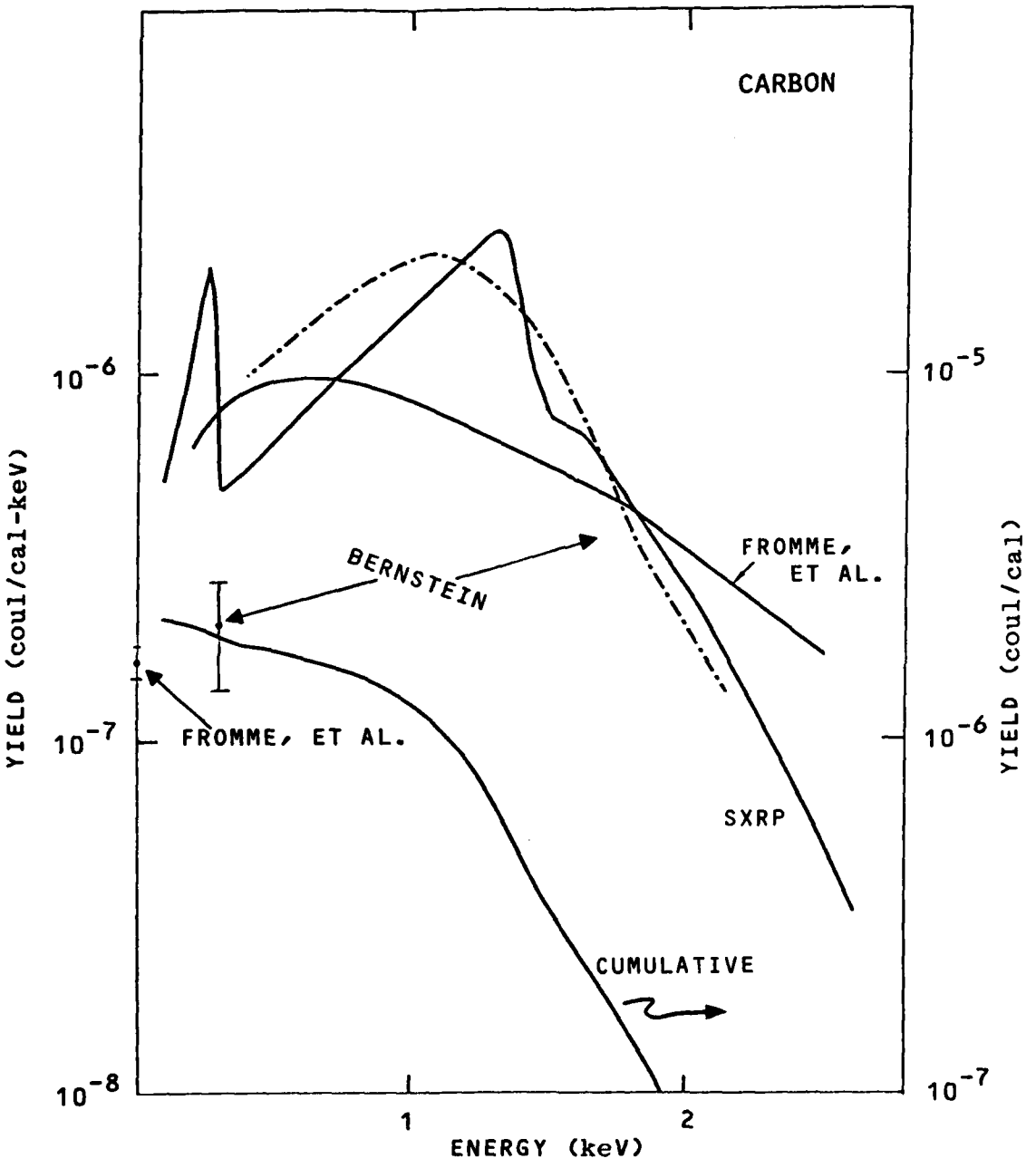

FIGURE 35. Calculated and Measured Photoemission Spectrum and Its Cumulative Back Yield for an EWR Source Incident on C.

TABLE 11. EWR PHOTOEMISSION YIELDS IN 10^{-5} coul/cal

MATERIAL	THIS WORK	BERNSTEIN	FROMME, ET AL.
Aℓ	1.5	1.3	1.8
$Aℓ_2O_3$	0.82		
Au	3.2	2.1	2.1
Ag	0.88	1.5	1.6
Cu	2.0	—	—
C	0.21	0.20	0.16

Section 4

USING BACK-BIASED DIODE DATA TO SPECIFY PHOTOEMISSION SPECTRA - II. GOLD

This is the second note concerned with the analysis by Fromme, et al.[11] of back-biased diode data for an exploding wire radiator source (EWR). Their analysis was applied to obtain an analytic representation of the photoemission spectrum. The first note was concerned with Aℓ and $Aℓ_2O_3$, and showed significant differences in the photoemission spectra as calculated using the SXRP code versus that deduced from the diode data.[4] It was concluded that the diode data do not contain the needed information to provide a realistic shape to the photoemission spectrum. A highly accurate diode current profile would be required since a double differentiation is necessary to obtain the photoemission spectrum.

We have carried out the Fromme analysis in reverse, as was done previously for Aℓ. Starting with the photoemission spectrum, a double integration (over emission angle and electron energy) is performed leading to electron current as a function of the applied bias voltage. This has been done numerically for the SXRP spectrum. In the Fromme analysis, analytic expressions are given for both the photoemission spectrum and diode current.

The analysis to follow is based on the original version of the paper by Fromme, et al. There, the yield and mean energy for the EWR source incident on Au were 1.2×10^{14} e/cal and 0.47 keV. These values have since

been replaced by the values 1.3×10^{14} e/cal and 0.60 keV. The differences have no effect on the conclusions drawn from this analysis. The calculated photoemission spectrum and that deduced by Fromme, et al. were previously presented in Figure 5. The Fromme spectrum is given by:

$$F(E) = Q_o \frac{E}{E_o^2} e^{-E/E_o} \text{ electrons/cal-keV} ,$$

with $Q_o = 1.2 \times 10^{14}$ electrons/cal and $E_o = 0.47$ keV. The results in Figure 5 apply to the same filtering of the photon spectrum, namely, 0.8 mils of kapton coated with 2000 Å of Aℓ.

A double integration of the photoemission spectra in Figure 5 over angle and energy leads to the results shown in Figure 36. The data give the collected charge at a given bias voltage and were taken directly from the paper by Fromme, et al. The dashed curve is Fromme's exponential fit to the data given by:

$$Q(E_b) = Q_o e^{-E/E_o} \text{ electrons/cal} ,$$

with the same Q_o and E_o previously specified. Two profiles corresponding to the calculated photoemission spectrum are shown. The unscaled curve is taken directly from the calculated spectrum in Figure 5. The scaled curve is simply shifted with respect to the first to provide a better comparison in shape with the data and with the exponential fit.

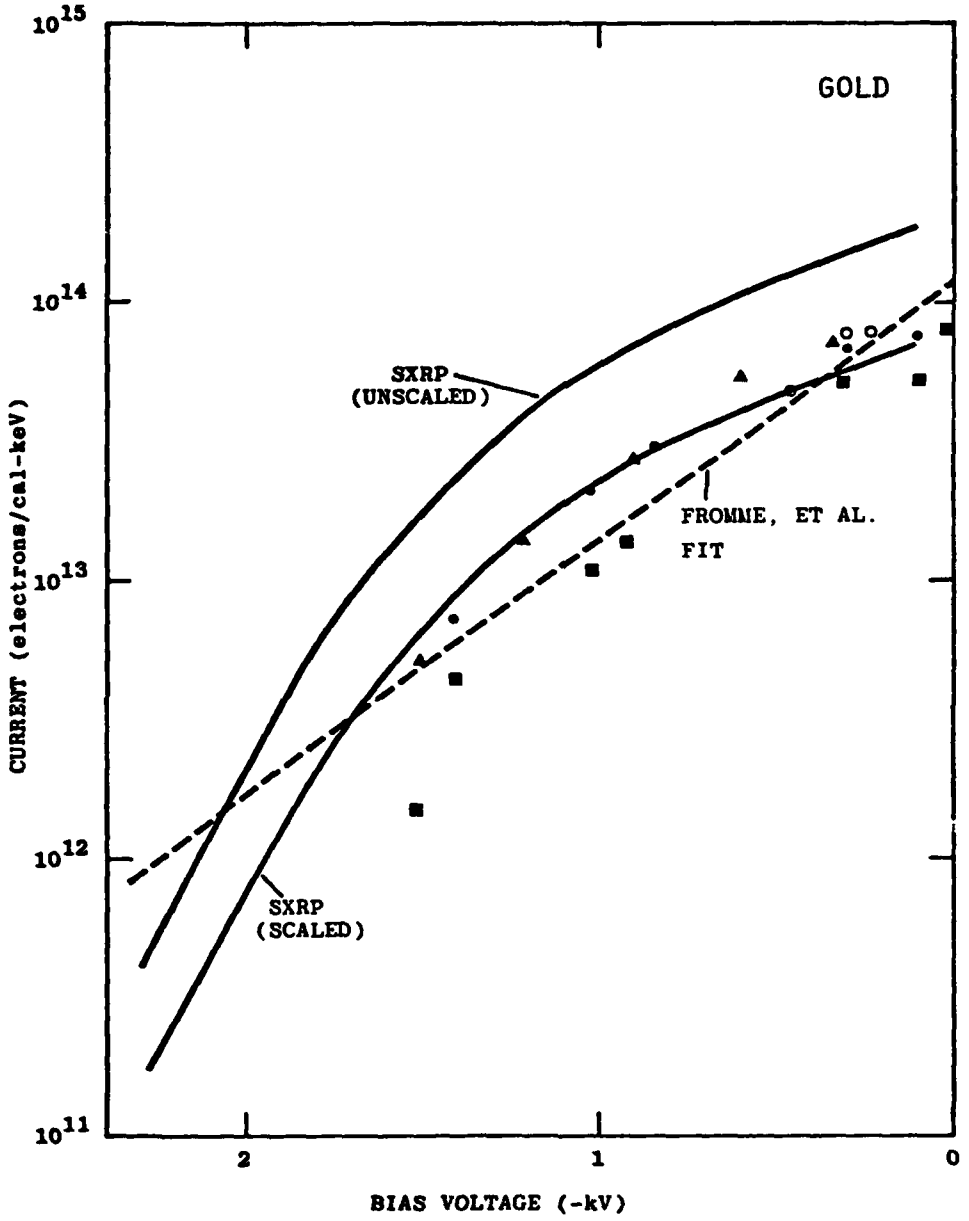

FIGURE 36. Diode Current Profiles and Data for an Exploding Wire Radiator Source Incident on Au.

One can appreciate the difficulty of deducing a good photoemission spectrum from diode data by examining the results in the figure. Either of the profiles can provide an equally good fit to the data and, yet, the associated photoemission spectra are significantly different from one another. The existing data simply do not contain the needed precision nor extend to a sufficiently high voltage to provide a reliable current profile. Furthermore, such a profile would be poorly represented by an exponential function since curvature does exist and critically affects the shape of the deduced photoemission spectrum. Individual sets of data do suggest curvature like that exhibited in the calculated profile.

Since both real shot-to-shot variations and uncertainties exist in the measured EWR source spectrum, we have examined the variation in both the calculated photoemission spectrum and resulting diode current to variations in the photon spectrum. The variations we considered have already been discussed in connection with Figure 9. The range of variation in the three photon spectra are well beyond the expected actual variation in the EWR source spectrum.

As previously discussed, Figure 9 shows the calculated photoemission spectra, while Figure 37 shows the resulting diode currents for the three photon spectra. The photoemission results have been discussed in Section 2 and thus our comments will be brief here. The total yields for the three cases are nearly the same because of the fortuitous circumstance for Au that the 1.65 keV feature and the broader higher energy continuum in the EWR source give essentially the same total yield. Although differences do exist in the

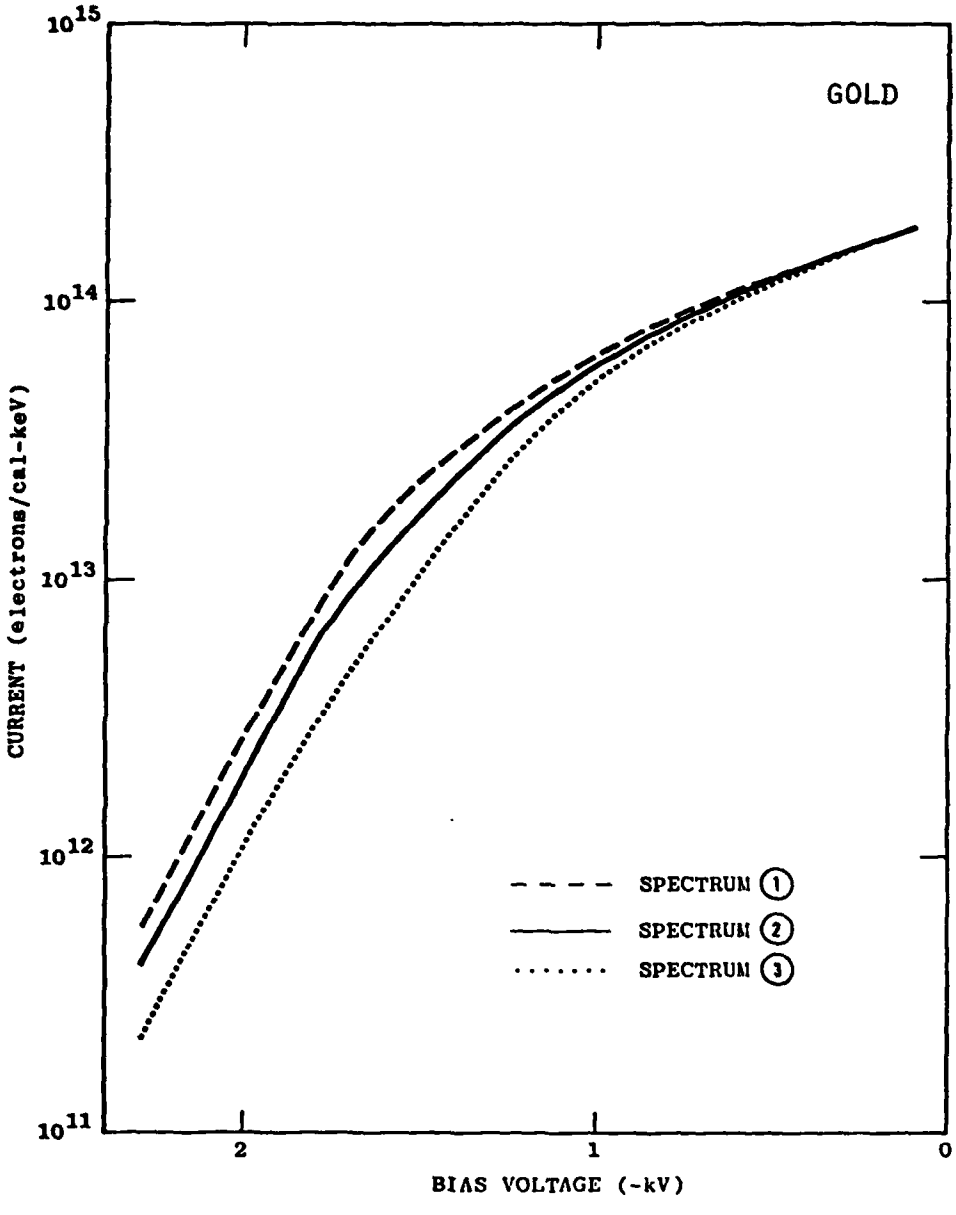

FIGURE 37. Diode Currents for the Photoemission Spectra Shown in Figure 9.

three diode currents which correspond to significant differences in the photoemission spectra, it would not be possible to select a best current profile among these based on the data. This illustrates again the severe problems of deducing a reasonable representation of the photoemission spectrum from a measurement of back-biased diode current.

REFERENCES

1. D. J. Strickland, D. L. Book, T. P. Coffey, and J. A. Fedder, J. Geophys. Res., 81, 2755 (1976).

2. D. J. Strickland, "Soft X-Ray Photoemission," RADC-TR-77-252 (July 1977).

3. W. L. Chadsey, B. L. Beers, V. W. Pine, D. J. Strickland, and C. W. Wilson, "X-Ray Photoemission; X-Ray Dose Enhancement," RADC-TR-77-253 (July 1977).

4. D. J. Strickland, D. L. Lin, T. M. Delmer, S. Rodgers, B. Goplen, and W. L. Chadsey, "Soft X-Ray Photoemission, II," DNA Final Report, submitted October 1977.

5. D. J. Strickland, IEEE Trans. Nuc. Sci., NS-24, No. 6, 2499 (1977).

6. D. J. Strickland, D. L. Lin, V. W. Pine, and W. L. Chadsey, "Soft X-Ray Photoemission and Charge Deposition Near Material Interface," RADC-TR-78-183, (August 1978).

7. D. J. Strickland and D. L. Lin, IEEE Trans. Nuc. Sci., NS-25, No. 6 (1978)

8. D. L. Lin, B. L. Beers, and D. J. Strickland, IEEE Trans. Nuc. Sci., NS-25, No. 6 (1978).

9. J. N. Bradford, IEEE Trans. Nuc. Sci., NS-20, No. 6, 105 (1973).

10. M. J. Bernstein, IEEE Trans. Nuc. Sci., NS-24, 2512 (1977).

11. D. Fromme, V. Van Lint, R. Stettner, and C. Mallon, Preprint July 14, 1977, and IEEE Trans. Nuc. Sci., NS-24, 2529 (1977). Some curves in the preprint are used in our comparison of photoemission spectra.

12. R. Haensel, C. Kunz, T. Sasaki, and B. Sonntag, Applied Optics 7, 301 (1968).

13. S. T. Manson, Phys. Rev. A6, 1013 (1972).

14. J. H. Hubbell, Atomic Data 3, 241 (1971).

REFERENCES (CONTINUED)

15. F. Biggs and R. Lighthill, "Analytical Approximations for X-Ray Cross Sections II," SC-RR-71-0507, Weapons Effects Research Department, Sandia Laboratories, Albuquerque, New Mexico (1971). E. Storm and H. I. Israel, "Photon Cross Sections from 0.001 to 100 MeV for Elements 1 through 100," LASL Report LA-3753 (1967).

16. H. Kanter, Phys. Rev. 31, 522 (1970).

17. P. W. Palmberg, T. N. Rhodin, J. Appl. Phys. 39, 2425 (1968).

18. M. Klasson, J. Hedman, A. Berndtsson, R. Nilsson, and C. Nordling, Physica Scripta 5, 93 (1972).

19. Y. Baer, P. F. Hedin, J. Hedin, M. Klasson, and C. Nordling, Solid State Commun. 8, 1479 (1970).

20. B. L. Henke, Phys. Rev. A6, 94 (1972).

21. C. J. Powell, Surf. Sci. 44, 29 (1974).

22. J. C. Ashley, C. J. Tung, V. E. Anderson, and R. H. Ritchie, "Inverse Mean Free Path, Stopping Power, CSDA Range, and Straggling in Aluminum and Aluminum Oxide for Electrons of Energy ≤10 keV," Report No. AFCRL-TR-75-0583 (December 1975).

23. B. P. Nigam, M. K. Sundaresan, and Ta-You Wu, Phys. Rev. 115, 491 (1959).

24. Handbook of Auger Electron Spectroscopy, Physics Electronics Industries, Inc. (1976).

25. K. Nielson, "Exploding Wire Radiation Source Support for SKYNET Phenomenology Experiments," Physics International (January 1977).

26. E. A. Burke, IEEE Trans. Nuc. Sci., NS-24, No. 6, 2505 (1977).

27. R. R. Schaefer, J. Appl. Phys. 44, 152 (1973).

28. H. Kanter, Ann. Phys., Lpz., 20, 144 (1957).

REFERENCES (CONCLUDED)

29. E. P. Savinov, A. P. Lukirskii, and Yu. F. Shepelev, Sov. Phys. – Solid State 6, 2624 (1965).

30. E. P. Savinov and A. P. Lukirskii, Optics and Spectroscopy 23, 163 (1967).

31. L. G. Eliseenko, V. N. Shehemelev, and M. A. Rumsh, Sov. Phys. – JETP 25, 211 (1967).

32. J. L. Gaines and R. A. Hansen, J. Appl. Phys. 47, 3923 (1976).

33. C. Kittel, "Introduction to Solid State Physics," 3rd ed., John-Wiley (1967).

34. J. C. Ashley, C. J. Tung, R. H. Ritchie, and V. E. Anderson, "Inverse Mean Free Path, Stopping Power, CSDA Range, and Straggling in Ni, Cu, Ag, and Au for Electrons of Energy ≤10 keV Calculated from a Statistical Model," RADC-TR-76-220 (1976).

35. D. C. Jackson, T. E. Gallon, and A. Chambers, Surf. Sci. 36, 381 (1973).

36. M. P. Seah, Surf. Sci. 32, 703 (1972).

37. M. P. Seah, J. Phys. F3, 1538 (1973).

38. J. C. Ashley, C. J. Tung, R. H. Ritchie, and V. E. Anderson, "Inverse Mean Free Path, Stopping Power CSDA Range, and Straggling in Polystyrene for Electrons of Energy ≤10 keV," RADC-TR-78-32 (1978).

DISTRIBUTION LIST

DEPARTMENT OF DEFENSE

Armed Forces Staff College
ATTN: Reference & Technical Services Branch

Assistant Secretary of Defense
International Security Affairs
ATTN: Policy Plans & NSC Affairs

Assistant Secretary of Defense
Comm. Cmd. Cont. & Intell.
ATTN: Dir. Survl. & Warning Systems,
W. Henderson

Assistant Secretary of Defense
Program Analysis & Evaluation
ATTN: Special Weapons & Support Systems Div.
ATTN: Strategic Programs

Assistant to the Secretary of Defense
Atomic Energy
ATTN: Executive Assistant

Defense Advanced Rsch. Proj. Agency
ATTN: DIR, Strategic Tech. Off.
ATTN: Director
ATTN: TIO

Defense Civil Preparedness Agency
ATTN: Hazard Eval. & Vul. Red. Div.,
G. Sisson

Defense Technical Information Center
12 cy ATTN: DD

Defense Intelligence Agency
ATTN: DT, J. Vorona
ATTN: DT-1, M. Fletcher
ATTN: DT-1B, E. Decker
ATTN: DB-4C, E. O'Farrell

Defense Nuclear Agency
ATTN: DDST
4 cy ATTN: TITL

Field Command
Defense Nuclear Agency
ATTN: FCPR

Field Command
Defense Nuclear Agency
ATTN: FCPRL

Joint Chiefs of Staff
ATTN: Director, Joint Staff
ATTN: J-5, R. Lawson
ATTN: J-3, E. Burkhalter
ATTN: SAGA/SFD

Joint Strat. Tgt. Planning Staff
ATTN: JLES, J. Enney
ATTN: JV, F. McMullen

Secretary of Defense Representative
Mutual & Balanced Force Reduction
DOD MBFR Task Force
ATTN: R. Clarke

DEPARTMENT OF DEFENSE (Continued)

National Defense University
ATTN: Classified Library

National Security Agency
ATTN: DIR, B. Inman
ATTN: D-9, J. Amato

Net Assessment
Office of the Secretary of Defense
ATTN: A. Marshall

Secretary of Defense
ATTN: Special Assistant

Undersecretary of Def. for Rsch. & Engrg.
ATTN: Strategic & Space Systems (OS)

DEPARTMENT OF THE ARMY

Deputy Chief of Staff for Ops. & Plans
Department of the Army
ATTN: DAMO-ZA, E. Meyer

Harry Diamond Laboratories
Department of the Army
ATTN: DELHD-N-P
ATTN: DELHD-N-TD, W. Carter

U.S. Army Materiel Dev. & Readiness Cmd.
ATTN: Commander

U.S. Army Nuclear & Chemical Agency
ATTN: Library

U.S. Army War College
ATTN: Library

DEPARTMENT OF THE NAVY

Naval Material Command
ATTN: R. Wertheim

Naval Surface Weapons Center
ATTN: Code X211
ATTN: Code F?i

Naval War College
ATTN: Code E-11

Nuclear Weapons Plans Policy & Reg. Br.
Plans Policy & Operations, OCNO
Department of the Navy
ATTN: NSP-10

Office of the Chief of Naval Operations
ATTN: OP 009
ATTN: OP 05
ATTN: OP 03
ATTN: OP 02
ATTN: OP 090
ATTN: OP 09, R. Long

Strategic Submarine Div.
Department of the Navy
ATTN: OP-21

DEPARTMENT OF THE AIR FORCE

Aerospace Defense Command
ATTN: Commander

Air Force Institute of Technology
Air University
ATTN: Library

Air Force Office of Scientific Research
ATTN: NA, B. Wolfson

Air Force Systems Command
ATTN: DL
ATTN: CC, A. Slay

Air Force Weapons Laboratory
Air Force Systems Command
ATTN: SUL
ATTN: CC, W. Lehman

Air University Library
Department of the Air Force
ATTN: AUL-LSE-70-250

Assistant Chief of Staff
Intelligence
Department of the Air Force
ATTN: INA

Assistant Chief of Staff
Studies & Analyses
Department of the Air Force
ATTN: AF/SA, J. Welch, Jr.

Deputy Chief of Staff
Operations Plans and Readiness
Department of the Air Force
ATTN: AFXO
ATTN: AFXOO
ATTN: AFXOX

Deputy Chief of Staff
Research, Development, & Acq.
Department of the Air Force
ATTN: AFRD
ATTN: AFRDQ

Foreign Technology Division
Air Force Systems Command
ATTN: SDBS, J. Pumphrey
ATTN: NIIS Library

Space & Missile Systems Organization
Air Force Systems Command
ATTN: CC

Space & Missile Systems Organization
Air Force Systems Command
ATTN: MN, J. Hepfer

Space & Missile Systems Organization
Air Force Systems Command
ATTN: RS, L. Norris

Strategic Air Command
Department of the Air Force
ATTN: DCS/OPS Plans
ATTN: DCS/Plans
ATTN: XPFS, L. Leavitt

DEPARTMENT OF ENERGY

Department of Energy
ATTN: Document Control for ET
ATTN: Document Control for ER-1, J. Deutch
ATTN: Document Control for OMA, D. Hoover

OTHER GOVERNMENT AGENCIES

Central Intelligence Agency
ATTN: OSR Registry

Federal Preparedness Agency
General Services Administration
ATTN: S. Schmidt

U.S. Arms Control & Disarmament Agency
ATTN: J. Young

DEPARTMENT OF ENERGY CONTRACTORS

Lawrence Livermore Laboratory
ATTN: L-001, R. Batzel
ATTN: L-203, L. Germain
ATTN: L-38, H. Reynolds

Sandia Laboratories
ATTN: Director
ATTN: R. Deurifoy
ATTN: Org. 5000

Sandia Laboratories
ATTN: T. Cook

DEPARTMENT OF DEFENSE CONTRACTORS

Aerospace Corp.
ATTN: W. Mann

AVCO Research & Systems Group
ATTN: J. Stevens

BDM Corp.
ATTN: J. Braddock

Boeing Co.
ATTN: V. Jones

Brookhaven National Laboratory
Technical Support Org. for Safeguards
ATTN: J. Indusi

Dougherty, R. E.
ATTN: R. Dougherty

G. A. Kent
ATTN: G. Kent

General Electric Co.
Re-Entry & Environmental Systems Div.
ATTN: C. Raver

General Electric Co.
Aerospace Grp. Strat. Planning & Prgms. Ops.
ATTN: R. Minckler
ATTN: D. Rodgers

General Electric Company-TEMPO
ATTN: DASIAC

DEPARTMENT OF DEFENSE CONTRACTORS (Continued)

General Research Corp.
ATTN: Technical Information Office

Henry S. Rowen
ATTN: H. Rowen

Hercules, Inc.
ATTN: Library

Institute for Defense Analyses
ATTN: J. Bengston

JAYCOR
ATTN: J. Young

Kaman Sciences Corp.
ATTN: A. Bridges

Lockheed Missiles and Space Co., Inc.
ATTN: Document Control

M.I.T. Lincoln Lab.
ATTN: L. Loughlin

University of Miami
ATTN: F. Kohler

Northrop Corp.
ATTN: D. Hicks

Pacific-Sierra Research Corp.
ATTN: F. Thomas

DEPARTMENT OF DEFENSE CONTRACTORS (Continued)

Pan Heuristics
Science Applications, Inc.
ATTN: A. Wohlstetter

R & D Associates
ATTN: C. MacDonald

Rockwell International Corp.
ATTN: J. Howe

Santa Fe Corp.
10 cy ATTN: D. Paolucci

Science Applications, Inc.
ATTN: J. Martin

Science Applications, Inc.
ATTN: D. Strickland
ATTN: D. Lin

System Planning Corp.
ATTN: J. Douglas

Systems, Science & Software, Inc.
ATTN: Document Control

TRW Defense & Space Sys. Group
ATTN: D. Scally

TRW Defense & Space Sys. Group
ATTN: J. Gorman